High-Fidelity Medical Imaging Displays

Aldo Badano
Michael J. Flynn
Jerzy Kanicki

Tutorial Texts in Optical Engineering
Volume TT63

SPIE
PRESS
Bellingham, Washington USA

Library of Congress Cataloging-in-Publication Data

Badano, Aldo.
High-fidelity medical imaging displays / Aldo Badano, Michael J. Flynn, Jerzy Kanicki.
p. cm. – (Tutorial texts in optical engineering ; TT63)
ISBN 0-8194-5191-6 (softcover)
1. Imaging systems in medicine. 2. Liquid crystal displays. 3. Cathode ray tubes. I. Flynn, Michael J. II. Kanicki, Jerzy. III. Title. IV. Series.

R857.O6B33 2003
616.07'54—dç22 2003056856

Published by

SPIE—The International Society for Optical Engineering
P.O. Box 10
Bellingham, Washington 98227-0010 USA
Phone: +1 360 676 3290
Fax: +1 360 647 1445
Email: spie@spie.org
Web: http://spie.org

Printed in the United States of America.

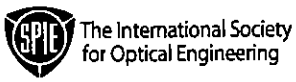

Contents

Chapter 5
Active-Matrix Organic Light-Emitting Displays

The dream is thus to put electronic circuit properties into single molecules. Arrays of such molecules – possibly connected by conductive-polymer wires – on molecular scaffoldings would form molecular wafers. One may speculate that reduced dimensions from 200 nm to, say, 2 Å, and the concomitant shrinkage in circuit size could increase the speed and dynamic memory of computers by a factor of 108. Such progress would correspond to forty years of computer technology development. Conductive polymers may become crucial for the building of such a molecular electronics world.

—B. Nordé and E. Krutmeijer in the announcement of the 2000 Nobel Prize in Chemistry to A. J. Heeger, A. G. MacDiarmid, and H. Shirakawa, for the discovery and development of electrically conductive polymers

5.1 Introduction to OLEDs

Organic light-emitting devices (OLEDs) are one of the most rapidly developing technologies in recent FPD history. Since the first appearance of OLEDs in the market as a monochromatic car stereo display in 1997, tremendous research from academia and industry has been performed to implement OLED-based display for low-cost, small to medium, FPD applications.[120] According to the OLED display industry's 2003 report of Stanford Resources and Strategies Unlimited, the worldwide OLED display market is expected to increase up to $2 billion (U.S.) by 2006.

OLEDs have several advantages over other FPD technologies: their Lambertian self-emission property[105] produces a wide viewing angle; their fast response time (below microseconds) is a benefit for moving images; their high luminous efficiency and low operation voltage guarantee low power consumption by the display; their

lightweight, very thin structure and robustness against external impacts are desirable characteristics for portable display applications; their simple, low-temperature fabrication process is cost effective; and their thin-film conformability on plastic substrates renders them a promising candidate for flexible display applications.[1, 88] Furthermore, when OLEDs are driven by an AM driving scheme based on TFTs, they can be used in high-resolution, large-size FPD applications such as laptop computers and TV screens. Recently, many companies—Toshiba and Matsushita,[158] Kodak and Sanyo,[101] Sony,[156] Samsung SDI,[145] and Chi Mei Optoelectronics and IBM Japan[159] have reported 15- to 24-in. active-matrix organic light-emitting display (AMOLED) prototypes with wide eXtended graphics array (WXGA) at 1200 × 768 resolution or eXtended graphics array (XGA) at 1024 × 768 resolution. The specifications of these prototypes are summarized in Table 5.1.

Table 5.1 Specifications of AMOLED prototypes.

Specification	Manufacturer				
	Toshiba and Matsushita	Kodak and Sanyo	Sony	Samsung SDI	Chi Mei Optoelectronics and IBM Japan
Screen Size (in.)	17	15	24.2	15.5	20
Resolution	WXGA/ 1280 × 768	WXGA/ 1280 × 720	XGA/ 1024 × 768	WXGA/ 1280 × 768	WXGA/ 1280 × 768
TFT Technology	poly-silicon	poly-silicon	poly-silicon	poly-silicon	amorphous silicon
Peak Brightness	300 cd/m^2	N/A	> 200 cd/m^2	N/A	500 cd/m^2
Emissive Material	polymer	small molecule	small molecule	small molecule	small molecule

5.1.1 History of OLEDs

Electroluminescence (EL) is the process of causing light emission from the radiative recombination of electrically created electrons and holes in organic materials. The discovery of EL of organic crystals can be dated back to the 1960s.[136] However, these early EL devices utilizing organic materials required several hundred volts and the light emission was inefficient.

During the late 1970s and early 1980s, the EL of organic thin films was advanced by reducing the operating voltage down to several tens of volts. This was achieved by subliming organic thin-films in a vacuum and using metal oxide electrodes.[139, 163] The efficiency of EL in organic materials was further improved

by new device configurations and new emissive materials. A charge-transport layer was inserted between the electrodes and the emissive material. Tang and Van Slyke observed efficient green light emission from 8-hydroxyquinoline aluminum (Alq_3) by inserting a hole-transporting layer (HTL) of aromatic diamine between the active material and the transparent ITO electrode.[155] In the 1990s, polymeric materials gained wide attention as strong candidates for light-emitting materials. Electroluminescence was observed in a layer of poly (phenylene vinylene) (PPV) sandwiched between two metallic electrodes when the device was sufficiently biased.[36] The EL in polymeric materials is from the radiative recombination of the singlet exciton across the π-π^* energy gap. Greenham et al. made a major breakthrough by inserting another polymer layer[69] having a band mismatch with the active polymer layer, causing the injected carriers to be trapped at the interface and resulting in an efficient charge recombination with a 20-fold enhancement of device quantum efficiency.

Overall, significant progress in OLEDs has been achieved in the last decade. Material advancement has enabled fabrication of white light,[98] blue light,[106] variable color,[26] and polarized EL devices.[53] The efficiency of OLEDs has also gained from material engineering. Typical examples include the use of phosphorescent organic material to enhance the internal quantum efficiency and the use of electrostatically self-assembled multilayers to reduce the hole injection barrier height for efficient carrier injection.[17, 81]

5.1.2 OLEDs for displays

After decades of research, OLEDs have exceeded their inorganic counterparts in light-emission performance. The light emission from OLEDs covers the full visible spectrum. They are inexpensive to fabricate and can be patterned on both planar and flexible substrates. Current research on LEDs made from organic semiconductors has shown high brightness and high power-conversion efficiency. Furthermore, displays made using OLEDs overcome many disadvantages associated with traditional LCDs. As discussed in Chapter 4, the disadvantages of LCDs include a narrow viewing angle and a slow response time of the LC molecules. Because OLEDs are emissive devices, components such as the backlight, polarizers, and top glass necessary in LCDs are not needed in OLED displays. OLED displays have a wide viewing angle, high brightness and contrast ratio, high visibility, light weight, and very thin structure. Moreover, the fast electronic response time and high luminescent efficiency associated with light-emitting organic materials allow high scan rates and low-power operation. All of these features make OLED-based displays very attractive.

5.1.3 OLED structures

A diode structure, in which the organic semiconductor is sandwiched between two electrodes, is the most commonly used scheme for LEDs (Fig. 5.1). It is speculated that the electrons in this configuration are injected into the organic material from a metal electrode (cathode), and holes are injected from the ITO electrode (anode) because ITO is n-type material. The authors think that electron extraction at the anode electrode is responsible for holes creation within organic layers. The injection of carriers from a metal into an organic material can generally be modeled by two theories: the Fowler-Nordheim (FN) model for tunnelling injection[65] and the Richardson-Schottky (RS) model for thermionic emission.[138, 148] The FN model considers the carrier injection as a process of carrier tunnelling from the metal through a triangular barrier into unbound continuum states, and ignores image charge effects that cause barrier lowering. The RS model assumes that a carrier from the metal can be injected once it has acquired enough thermal energy to surmount the potential maximum that results from the superposition of the external and the image charge potential.

Inelastic scattering of the carriers before travelling through the barrier maximum and tunnelling effects are not considered. However, in a real LED, the maximum of the electrostatic potential is located several nanometers away from the interface.[3] Ignoring this significant barrier lowering at the interface in the FN model makes it problematic. For organic light-emitting solids, the inelastic carrier scattering inside the potential well is important and cannot be ignored. This makes the application of the RS model insufficient to account for the physical process of carrier injection. Due to these deficiencies in the FN and RS models, Arkhipov et al. have come up with a theory that describes injection in similar terms as photo-conduction in organic solids. In the first step, charge and image charge pairs close to the inter-

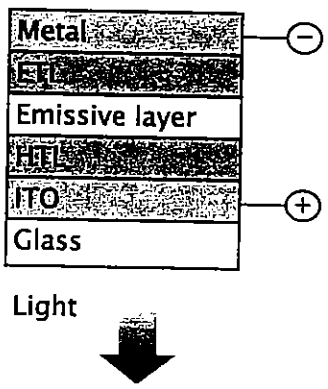

Figure 5.1 Schematic of an OLED. An ITO electrode is used for hole injection, and a metal electrode is used for electron injection. The emissive organic material is separated from direct contact with the electrodes by a hole-transport layer (HTL) and an electron-transport layer (ETL).

face between the electrode and the organic are generated with the assistance of temperature and electric fields. The pair can fully dissociate in the course of a diffusive process, which is also temperature- and field-assisted. The model calculation generates results in good agreement with experimental results.[3] In order for the carriers to be efficiently injected, the contact between the electrode and the organic are made ohmic, which has a Schottky energy barrier of less than about 0.3 eV.

After the two types of carriers (electrons and holes) are created within the devices, they will drift/diffuse and recombine with each other along their diffusion pathway. The mobility of carriers plays an important role in the light-emission process. If the mobility is very low—much smaller than the 1 cm^2/Vs that is typical for organic semiconductors—the injected carriers pile up near the interface between the electrodes and the organic, and the radiative recombination rate is slow. For an optimized device, the electron and hole creation and transport should be balanced for a maximum recombination current and the highest power-conversion efficiency. A model that takes into account charge injection, transport, recombination, and space charge effects in organic materials has yielded an accurate solution for LEDs, with ohmic contacts for both electron and hole injection and high-mobility materials for balanced carrier transport.[47] In order to overcome the low carrier mobility of organic semiconductor materials, practical LED devices contain an ETL and an HTL that separate the light-emitting layer from direct contact with the electrodes. Figure 5.2 summarizes the typical internal quantum efficiency achieved by selecting electrode and carrier transport materials.[71]

Even though the emission efficiency is enhanced by incorporating electron- and hole-transport layers, other factors such as carrier injection for blue light emission are still problematic due to the large band mismatch between the electrodes and organic materials, especially for hole injection. Efficient electron injection can be achieved by choosing low work function metals, such as Ca. For electron extraction (or hole injection), one of the most suitable candidates is ITO (a high

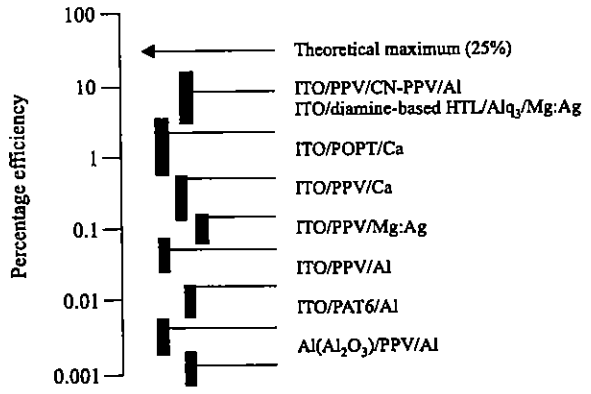

Figure 5.2 Typical internal quantum efficiencies for OLEDs. Reprinted from Ref. [70] with permission of Elsevier.

work function metal) for better light-emitting devices. However, by novel molecular-scale interface modification through self-assembly, the carrier injection efficiency of ITO can be significantly improved.

In order to grow these electro-statically self-assembled layers, solutions of polymeric ions are needed. The substrate on which the films will be grown is preprocessed to have surface charges. The substrate is alternately dipped into the polycation and the polyanion solutions to form the ionic-attracted polymer layers. Ho et al. have devised a smart design of interface layers to control carrier (especially hole) injection to achieve high EL efficiency in polymer OLEDs.[81] The goal of the ITO surface modification is to form stepped and graded electronic band profiles between the electrode and the light-emitting polymer. It turns out that partially de-doped poly(3,4-ethylenedioxythiophene): poly(4-styrenesulphonate) (PEDT:PSS) composites have different ionization energies. To fabricate the graded profile, PEDT:PSS composites are de-doped by hydrazine (N_2H_4) into different levels. The ITO surface normally contains negative charge in solution due to dangling oxygen bonds. By alternately dipping ITO substrate into polycationic poly(p-xylylene-α-tetrahydrothiophenium) (PXT) solution and polyanionic PEDT:PSS solution with various doping levels, an interface HTL forms. The final structure and schematic diagram of the band profile of the interface layer are shown in Fig. 5.3. The abrupt hole-injection (or electron-extraction) barrier between the ITO and the light-emitting polymer are graded into several smaller barrier heights, which permit a much easier carrier extraction from the light-emitting polymer. Such a scheme is expected to be especially useful for blue light-emitting polymers with large ionization energies. A green-emitting LED fabricated using this method yielded a 6% external efficiency at a luminance of 1600 cd/m^2 and at a bias of 5 V. Another approach to produce a similar effect is the insertion of the HTL between the ITO/PEDTiPSS interface and the light-emitting layer (LEL). The bandgap of HTL is larger than LEL.

There is another factor that limits the theoretical maximum internal quantum efficiency to 25%. When an organic material becomes excited through the optical energy gap, it returns to ground state by two mechanisms: fluorescence and phosphorescence. These two radiative processes share the same general mechanism but involve different excited states. A singlet state refers to a two-paired electron hole with opposite spins. A triplet state refers to a two-paired electron hole with the same spin. Fluorescence involves the transition from an excited singlet state to a singlet ground state, and phosphorescence is the transition from an excited triplet state to a singlet state.[3, 17]

In OLEDs, the injected carriers have spins, hence their means of recombination determine the spin configuration of the exciton (electron-hole pairs). Only 25% of the generated excitons are in singlet states and can emit light, while the other 75% become triplet excitons and decay through nonradiative pathways. This puts a physical limitation on the internal quantum efficiency that can be achieved in normal OLEDs. Baldo et al. have come up with a solution to harness the triplet excitons to emit light by transferring excitonic energy from a host material to a phosphorescent molecule and then to a fluorescent molecule that emits light.[17]

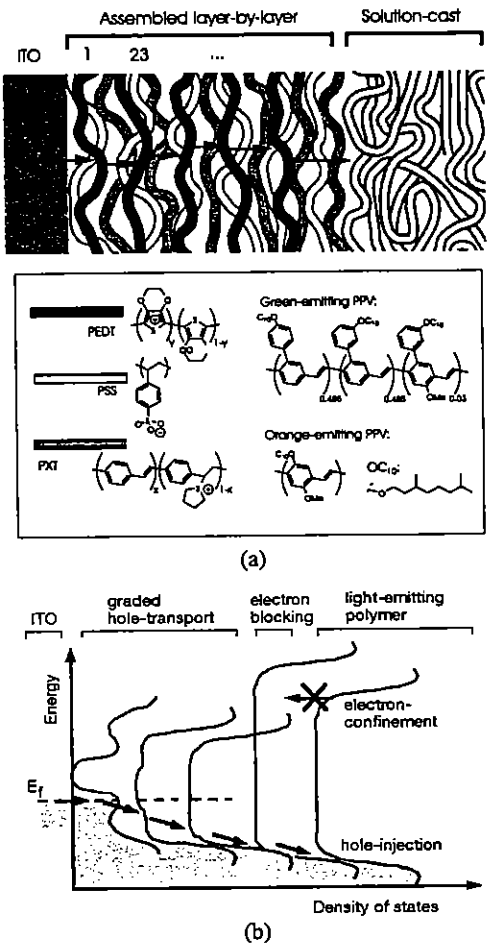

Figure 5.3 (a) Schematic of the hole-injection interlayer between the ITO electrode and the light-emitting polymer (top), and the chemical structures of the polymer (below). The interlayer consists of five graded bilayers of PEDT:PSS/PXT films plus one PSS/PXT bilayer formed by electrostatic self-assembly technique. (b) Schematic of electronic density of states across a graded interlayer. Occupied states are shaded. Holes are transported to the light-emitting material through graded lower effective barrier layers. An electron-blocking sublayer fabricated from a lower-electron-affinity polymer is also shown. Reprinted from Ref. [81] with permission of Nature/Macmillan.

There are two primary mechanisms for the energy transfer. One, called Dexter transfer, occurs over short distances and requires contact between the donor and acceptor molecules. During the transition, the exciton retains its spin configuration. Such an energy transfer is useless in terms of improving internal quantum efficiency, since triplet excitons are still forbidden to emit light. The second energy transfer pathway is called Förster transfer and can change the exciton spin configuration. This transfer does not require contact and can occur over a long distance. The different interaction ranges of the two energy transfer processes can be exploited to

minimize Dexter transfer while maximizing Förster transfer. This situation can be realized by placing the phosphorescent and fluorescent molecules in alternating layers of the device. This can give an internal efficiency of fluorescence as high as 100%. The fabricated fluorescent red OLED quadruples the device efficiency. The increased efficiency reduces heating during light emission in the device and extends the lifetime of the device, since high luminance can be achieved at lower current density.

5.1.4 EL organic materials

The properties of organic light-emitting materials are different in comparison with the traditional inorganic semiconductors. Table 5.2 offers a comparison of inorganic semiconductors with polymeric light-emitting semiconductors.[71] There are two major categories of EL organic semiconductors: small molecules such as Alq_3, and polymers such as PPV. The two categories have in common an extended region of alternating single and double bonds in a carbon chain. In these regions, electrons form covalent bonds evenly distributed—an effect known as "conjugation." Electrons move more freely within the conjugated segments that are flat and rigid. Conjugated materials have distinctively strong coloration because these p-electrons can absorb light in the visible range. Conjugated regions can be affected by extra charge introduced to or removed from the polymer chain by chemical doping or charge injection (or extraction). Charge injection (or extraction) thus gives rise to a change in absorption as the molecule slightly rearranges itself. The color of emission is dependent on the positions of the atoms in the excited molecule, which may be different from the ground state. Some common organic light-emitting materials and their emission wavelengths are shown in Fig. 5.4.

Before the discovery of light-emitting polymers, small molecules such as 8-hydroxyquinoline Al were studied extensively for OLEDs . These materials are easy to purify and can be sublimed directly onto the device in a vacuum. Today, polymers are becoming preferred in device applications since they are expected to be more stable, particularly at high temperatures, and easier to process over large areas. There are two types of polymers used in OLEDs: precursor and soluble. Insoluble polymers, such as PPV, must be deposited in precursor form.[36] PPV precursors are soluble in methanol and water and are readily spin-coated as a thin film onto an ITO-coated substrate. Heating then converts the precursor into the fully conjugated polymer form.

The relative inertness and insolubility of the polymer make it particularly useful for multilayered devices. MEH-PPV is an example of a soluble, conjugated emissive polymer.[169] The large side-groups attached to the phenyl ring cause the polymer to be soluble in common organic solvents such as chloroform, toluene, and xylene. These bulky side-groups also make the polymer more amorphous and affect the color of the films by contributing to the conjugation of the whole molecule. Both precursor and soluble polymers offer advantages for inexpensive large-area, thin-film deposition. Some of their properties such as color, mechanical strength,

Table 5.2 Comparison of traditional and polymeric semiconductors.

Feature	Traditional Semiconductor	Polymeric Semiconductor
Band gaps	Si 1.1 eV Ge 0.67 eV GaAs 1.35 eV Relatively sharply defined	poly(acetilene) 1.4 eV PPV 2.2 eV MEH-PPV 2.1 eV Varies with polymeric segments: these are minimum band gaps
Conductivity σ Ω^{-1} cm^{-1}	Doped silicon 1 Intrinsic Si 0.0001	PPV 10^{-14} Doped poly(acetylene) max. 10^{4}
Doping	$<10^{20}$ cm^{-3} in crystal structure	Up to $<10^{22}$ cm^{-3} in interchain sites
Typical dopant	P, As, Sb, B (IV materials) Zn, Si (III-V materials)	I_2, AsF_5, $SbCl_5$, $FeCl_3$, O_2
Mobility μ (cm^{2}V^{-1}s^{-1})	>1000 single crystal α-Si 0.1–10	poly(acetylene) $>10^{-3}$ PPV $<10^{-8}$
Density ρ (g cm^{-3})	Si 2.33 Ge 5.32 GaAs 5.32	PPV 1.24
Preparation	Grown from melt, sawn, and polished	Deposited from solution as thin film (polymer) or vacuum sublimed (small molecule)
Morphology	Single crystal	Disordered with tendency for molecules to lie parallel to substrate
Purity	Very high	Polymer: low Sublimed molecules: high
Transport	3D	Quasi-1D with 3D hopping to neighboring chains
Charge	Electrons and holes	Electrons and holes localized as polarons or bipolarons
Temperature dependence	$\sigma \sim e^{-\Delta\varepsilon/kT}$	$\sigma \sim e^{-A/T^{1/M}}$ (Mott hopping)
Stability	Good Diffusion of dopants High temperatures	Poor Prone to photo-oxidation Permeable to gases
Surfaces	Dangling bonds	No dangling bonds
Bulk	Covalent bonding	Molecules held by weak Van der Waals forces Atoms held covalently
Refractive index	Si 3.4 GaAs 3.6 In GaAs 3.5	PPV is anisotropic: 2.2 and 1.7

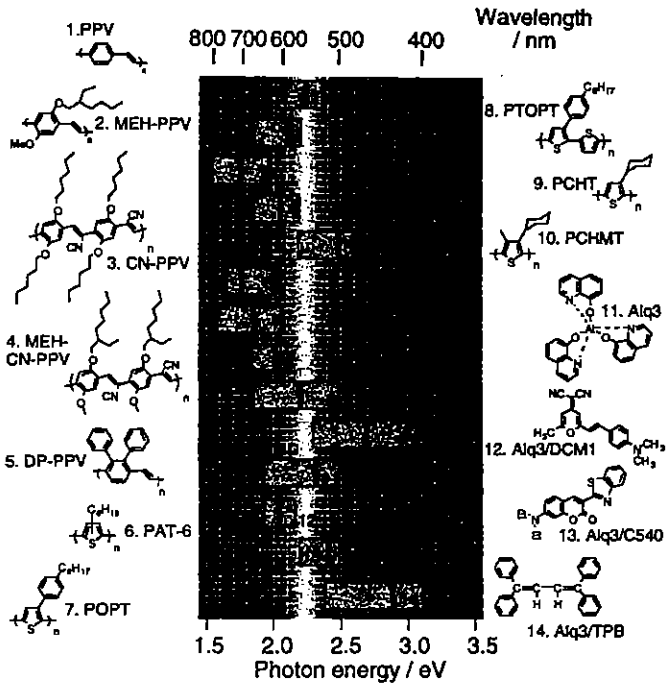

Figure 5.4 EL emission at full width, half maximum (FWHM) of a typical polymer and small-molecule light-emitting materials. Reprinted from Ref. [71] with permission of Elsevier.

and efficiency can be engineered by chemistry and processing conditions.[35] Polymer blends and copolymers with active side-chains provide a versatile way to modify properties of light-emitting polymers. Unlike PPV or MEH-PPV, which have conjugation extended along the entire polymer backbone, active segments may be incorporated into an inert polymer either in the main chain or attached as side chains.[107, 170] The material will have most of the properties of the parent polymer rather than these active segment molecules. The weakening of the EL effect due to dilution of the active segments can be balanced by an increase in quantum efficiency that arises from an increased separation between active regions.

The biggest hurdle for OLED application in consumer-grade displays lies in the potential instability of the device. Device properties may degrade in a complicated manner as a result of exposure to light, water, and oxygen molecules. The mechanisms of property degradation include the corrosion of contacts, the presence and migration of impurities, and the emissive material degradation. In most cases devices fade with time but maintain the same spectral distribution. On a microscopic level, dark spots and regions often appear, corresponding to pinholes and exposed edges of the cathode electrodes. Higher temperatures promote degradation and catastrophic failure, and are sometimes associated with local "hot spots." More details on device stability and encapsulation will be discussed later in this chapter.

5.2 Evaluation of Device Opto-Electronic Performance

Since different OLED materials and device structures affect device performance, it is necessary to characterize the OLED light output properties in order to develop high-performance OLEDs. The most common parameters that are used to describe the device performance are luminance (cd/m^2), luminous efficiency (lumen/watt), emission efficiency (cd/A), quantum efficiency, and lifetime. The brightness of OLEDs determines its application range, and the device luminous efficiency indicates the power conversion ratio and the power consumption of the device.

It is known that the emission from OLEDs is close to a Lambertian emission, especially for small angles from the normal direction to the device surface. During the evaluation of the total luminous flux of the device, it is important to have a very small surface area at the detector and a large separation between the detector and the emissive surface in order to utilize the integration of Lambertian profile to get the total luminous flux. A silicon photodiode can be used as a detector. However, a silicon photodiode cannot resolve spectra, and thus can only be used in measuring the total luminous flux and luminance of the emissive device. In order to obtain the spectral distribution of the radiant power, luminance, luminous flux, and photon emission, a calibrated spectrometer must be used. The resulting spectral curves represent the complete properties of the light emitted from the source, but also provide an accurate description of the physical properties of the device such as the EL external quantum efficiency. It is convenient to use a CCD camera to capture the spectral information of the emitted light.[75] The CCD camera needs to be carefully calibrated because the CCD's spectral response is different at different wavelengths, and this effect needs to be considered during the processing of the acquired spectral response. Once this spectral distribution of energy is obtained, the external quantum efficiency can be calculated using

$$\eta_e = \frac{N_{photon}}{N_{electron}} = \frac{\int P(\lambda) sp(\lambda) d\lambda}{J/e}, \tag{5.1}$$

where $sp(\lambda)$ is the measured spectral response from the CCD, $P(\lambda)$ is the calibration spectra of the CCD, and J is the applied current density.

5.3 Device Configuration and Display Fabrication

In this section, we discuss some of the OLED pixel and subpixel structures and fabrication processes that have high potential to be used in full-color FPDs. We begin with the basic structure of a conventional OLED and then move to more exotic pixel structures.

5.3.1 Conventional OLED

The basic structure of a conventional OLED is shown in Fig. 5.5(a). A minimum of two thin-film organic layers is required. The first layer is the HTL, and the second layer is the electron-transporting, light-emitting layer. In some cases, a third organic thin-film is used, as in Fig. 5.5(b). For this structure, the first layer is the HTL, the second thin-film is the LEL, and the third layer is the ETL. In each case, the bottom, hole-injecting (or electron-extracting) electrode is usually made of conductive ITO sputtered onto the glass substrate. The ITO electrode is transparent to visible light, and therefore, light is emitted through it when the OLED is forward-biased. The top, electron-injecting electrode (cathode) is usually a vacuum-evaporated, low work function metal or metal alloy such as Mg-Ag or Li-Al.[38] The organic layers consist of proper combinations of either small organic molecules or organic polymers. In the case of small molecules, the thin films are deposited by thermal evaporation in a vacuum. For the polymer-based OLEDs, the preferred method of deposition is spin-coating or ink-jet printing. This is a bottom light-emitting device structure. Since most of the organic materials used are sensitive to air,

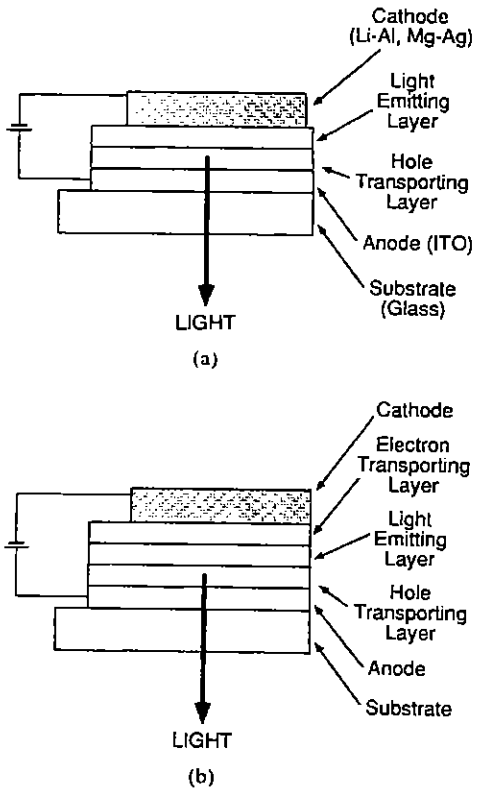

Figure 5.5 Conventional OLED structure. Reprinted from Ref. [38] with permission of the IEEE.

some form of encapsulation or passivation is usually required to reduce degradation by the formation and growth of dark-spot defects.[103]

5.3.2 Side-by-side subpixels

Figure 5.6(a) shows a side-by-side individual R, G, and B subpixel scheme, which resembles CRT arrangements. In this simple approach, each OLED subpixel requires a different light-emitting organic material. Therefore, arrays of each type of OLED must be deposited and patterned independently. This requirement may give rise to problems; for example, the patterning of one of the organic layers can cause a previous layer to swell due to the organic solvents used in the photolithographic processes, or to deteriorate due to the relatively high processing temperatures used in the etching process.[38] However, by using the side-by-side pixel scheme, 300-dpi displays have been fabricated.[38]

Some fabrication techniques can be used to overcome these limitations. One technique, described by Burrows et al.,[38] uses dielectric "walls" that have been patterned on the substrate to separate each subpixel and to shadow two of the three subpixels from the unwanted thermal deposition of the light-emitting material. By tilting the substrate for each of the three organic layer growths, R, G, and B organic material can be grown in separate areas, thereby providing three distinct subpixels. However, nonuniformity can result from the difficulties of controlling the deposition area. Another technique is the precision shadow-mask method. In this approach, selective deposition of R, G, and B organic materials is done with a thin mask and a high-accuracy mask-moving mechanism. To obtain good patterning and better size control, the mask should be thin and the distance between the mask and the substrate should be as small as possible. Unfortunately, due to the thin mask requirement, difficulties arise because the mask must be kept flat, which leads to a nonuniform gap between the mask and the substrate. This is especially true for large-area substrates. In the side-by-side subpixel technique, the light emission from each subpixel is controlled independently and can be optimized separately to reach higher quantum and power efficiency. In summary, the unevenness of the mask, nonuniform gaps, and nonuniformity caused by oblique deposition hinder this technique from its use for large-area display fabrication.

5.3.3 White OLED filtering

Figure 5.6(b) presents another pixel scheme that can be used to realize a full-color display. This color subtraction scheme can be compared to LCDs in that the white OLED serves as a "backlight" and the emitted light is passed through separate R, G, and B filters. The white OLED is fabricated by deposition of two or more organic layers that emit different colors (R, G, and B) onto a prepatterned substrate. The thickness of each organic layer is such that the superposition of the light emit-

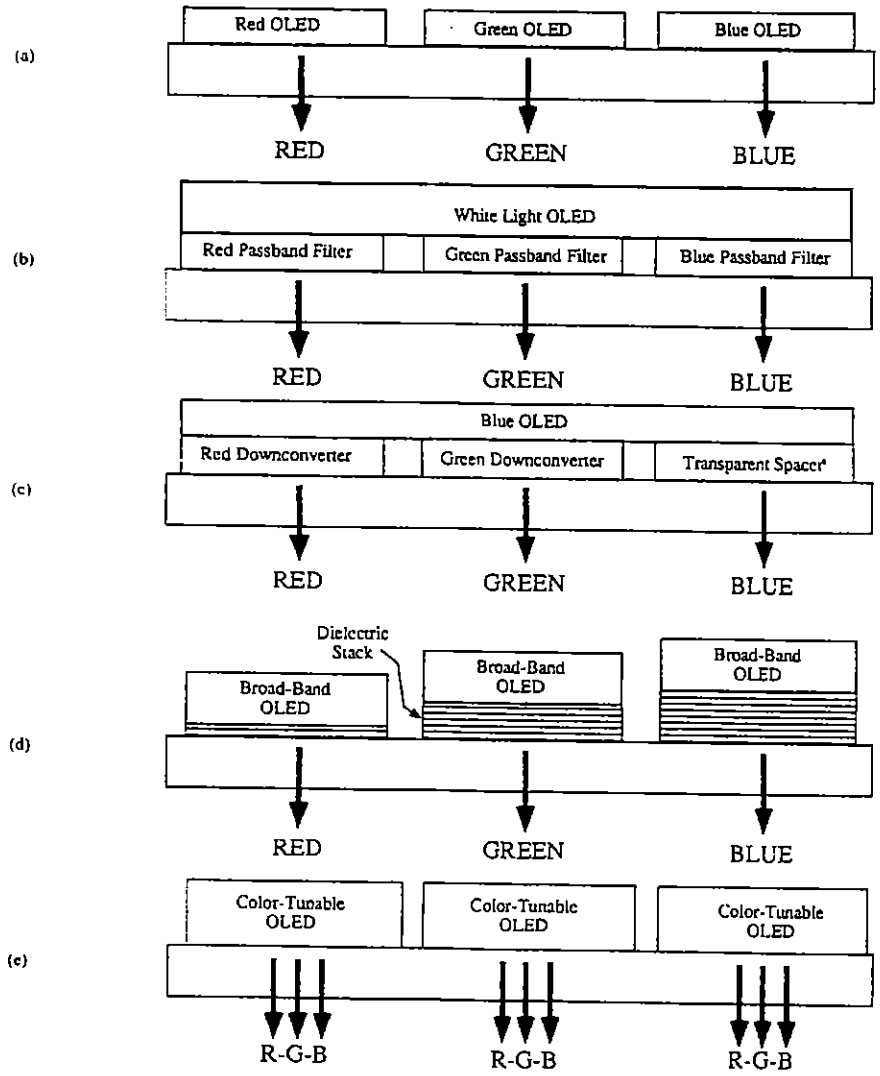

Figure 5.6 Five full-color subpixel configurations. Reprinted from Ref. [38] with permission of the IEEE.

ted appears white. No post-deposition patterning is required since only one white OLED structure is grown over the entire substrate.[70] However, this pixel design approach has limitations. The main disadvantage is that most of the emitted light (up to 90% of the optical power) is absorbed by the filter to achieve a fully saturated color subpixel. This requires the OLED to be driven at a higher current density to achieve sufficient brightness. Unfortunately, a high current density produces more defects and heat, and accelerates OLED degradation.[38] Even with these limitations, white OLED filtering is still a viable technique that can be used in the fabrication of FPDs where power consumption is not a major concern, but good device stability is required.

5.3.4 Blue OLED down-conversion

Figure 5.6(c) illustrates a photoluminescent method to realize separate R, G, and B subpixels. A blue OLED is used to optically pump a prepatterned subpixel, which consists of a fluorescent material that absorbs the blue light and emits either red or green light. For blue light, a transparent layer (spacer) is used in place of the red or green fluorescent organic material. Even though the power efficiency of this system can be low because the energy of the emitted red or green photon is less than the energy of the absorbed blue photon, the conversion quantum efficiency (photons out/photons in) can be near 100%.[38]

A major problem with this technique is the guiding of light, by the substrate, into the neighboring subpixels, causing unwanted photoluminescence. This is a form of optical crosstalk and causes color bleeding in the subpixels, which reduces the contrast of the display. Burrows et al. have demonstrated that the substrate guiding of the light, and therefore the color bleeding, can be reduced by using a shaped substrate that enhances forward light scattering.[38] For example, the structure shown in Fig. 5.7(b) greatly improves the output coupling of light, as compared to the structure in Fig. 5.7(a).

5.3.5 Microcavity OLEDs

Figure 5.6(d) shows the use of microcavity filters to realize R, G, and B subpixels based on an inherently broadband OLED. Microcavities have been shown to be an effective method to control the direction and color of OLED emissions. The microcavity is formed by the reflective metal electrode on the top of the OLED and a dielectric, quarter-wavelength, multilayer structure that has been fabricated under the transparent ITO in the bottom of the structure. When a white OLED is placed in this cavity, the OLED will emit light of a certain color in a certain direction.[38] In this approach, the emission's spectral bandwidth becomes narrower and the intensity is enhanced due to the microcavity effect. Under careful design (i.e., changing the length of the cavity), it is possible to position the emission in the desired wavelength band. The increase of emission intensity reduces the required driving current, thereby reducing power consumption. Thus, degradation of OLEDs is reduced and lifetime increases.

This technique does have two main limitations. The first is the directional dependence of the wavelength selection. In other words, different colors are preferentially seen at different angles from the microcavity OLED structure. Typically, the viewing angle is around 15 deg for a 10:1 luminance decrease. Secondly, the different microcavity structures for R, G, and B create a wide variation in thickness, and this thickness is usually larger than the organic layer. Therefore, it is difficult to deposit a continuous, high-quality organic light-emitting layer on the substrate containing the prepatterned microcavity structures.[38] Microcavities are, however, an important means of tuning the color of the emitted light.

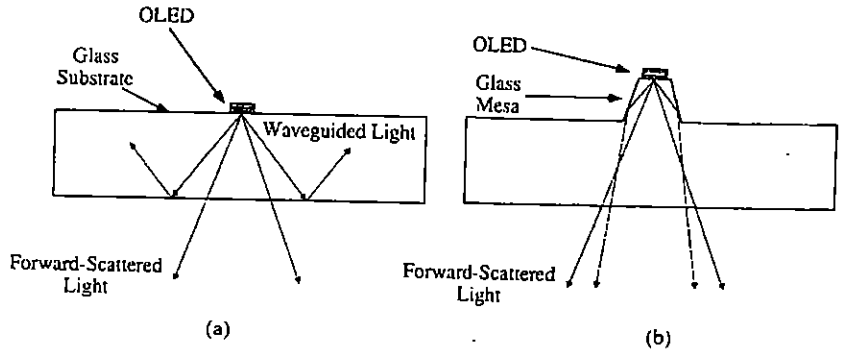

Figure 5.7 Schematic cross-section of an OLED grown on (a) a plain substrate, and (b) a mesa-shaped substrate. Reprinted from Ref. [38] with permission of the IEEE.

5.3.6 Color-tunable OLEDs

Figure 5.6(e) illustrates the concept of using a single, color-tunable OLED. This scheme eliminates the need for individual R, G, and B subpixels to create one full-color pixel, which results in an enhancement of the display resolution and pixel fill factor by a factor of three compared to previously discussed pixel schemes.[63] Due to the fact that only one OLED configuration is grown over the entire surface, the need for prepatterning the substrate is removed, thereby providing a simpler fabrication process. However, this advantage trades off with the requirement of more complex driving circuits, because the circuit must be able to control simultaneously the color, brightness, and gray level of the OLED. One method that has been used to achieve a color-tunable OLED involves a polymer blend or polymer electrochemical cell as the light-emitting organic material. Each ingredient of the blend or cell emits at a different wavelength. The color and brightness (gray level) can be tuned by applying different voltages and/or a different polarity to the OLED, i.e., high voltage pushes the emitted color into the blue region and lower voltage corresponds to more red light emission. However, the higher voltage also causes higher current injection, and therefore affects the brightness of the OLED.[38] This method also has problems achieving full color due to the ever-present lower energy light emission regions and possible accelerated degradation of the OLED at high current levels.

5.3.7 Pyramid-shaped pixel OLEDs

The idea of using pyramid-shaped pixel OLEDs to achieve color has been published recently.[168] In this technique, different organic materials, emitting different colors, are deposited on each surface of a pyramid-shaped structure. The basic concept is similar to that of side-by-side subpixels, but this approach provides a three-fold enhancement in the resolution because three subpixels are integrated

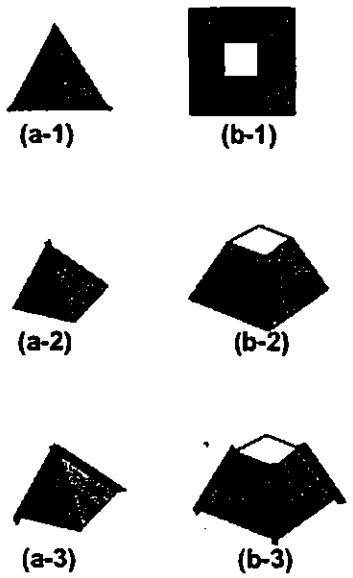

Figure 5.8 Different structures of pyramid-shaped pixels. Diagrams (a-3) and (b-3) show the dielectric mask wall. Reprinted from Ref. [168] with permission of the American Institute of Physics.

into one pixel. The fabrication processes seem to be relatively easy and require oblique thermal deposition of organic materials. As different materials are deposited, only a rotation of the samples is needed. Thus, this process requires no mask. The different pyramid structures that can be used are shown in Fig. 5.8. To guarantee that proper materials are deposited on the correct surfaces, a dielectric mask wall on the edges is fabricated before evaporation, which provides better shielding. In addition to the aforementioned advantages, the pyramid-shaped structure also largely enhances the extraction quantum efficiency and reduces the optical waveguiding effect. A demonstration by use of an optical prism to simulate a pyramid-shaped structure is shown in Fig. 5.9.

Although this technique has many advantages, pyramid-shaped substrates are needed, which complicates the fabrication process and increases cost. Furthermore, due to the pyramid shapes, the viewing angle is limited. At least one color is blocked by pyramid structures at large off-axis viewing angles. The electrical connections and addressing scheme are also challenging. A more promising method to implement a color-tunable device is the stacked OLED.[64]

5.3.8 Stacked OLEDs

Stacked OLEDs (SOLEDs) have the potential to provide the highest image resolution simultaneously with low fabrication costs. As depicted in Fig. 5.10, the SOLED consists of a stacked blue OLED, green OLED, and red OLED. Most organic mol-

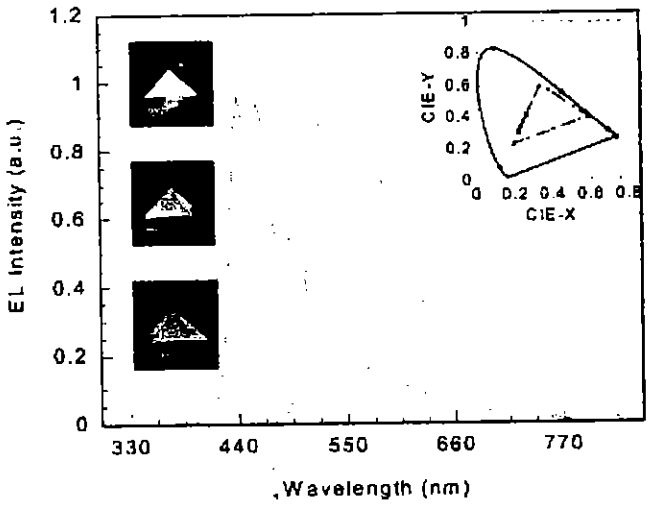

(a)

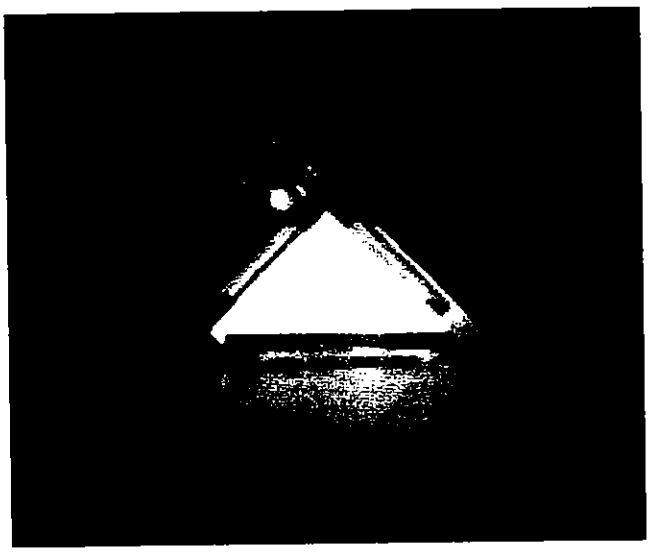

(b)

Figure 5.9 (a) Measured spectra of R, G, and B elements. (b) Picture shows white light emission as R, G, and B are turned on simultaneously. Reprinted from Ref. [168] with permission of the American Institute of Physics.

ecules and polymers on which these OLEDs are based have an emission spectrum that is red-shifted from the absorption spectrum. This property causes OLEDs to be transparent to their own emitted light and to most of the spectrum of visible light, giving rise to the transparent OLED (TOLED). Therefore, TOLEDs can be stacked on top of each other with only a small reduction in efficiency.

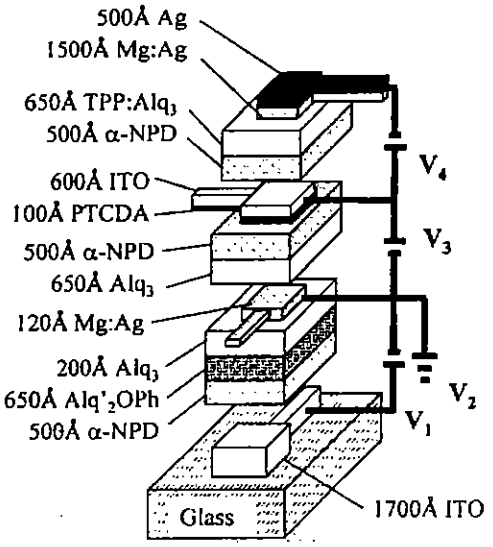

Figure 5.10 Stacked OLED (SOLED). Reprinted from Ref. [38] with permission of the IEEE.

The fabrication process to form this structure is relatively simple and does not involve etching of the organic materials. A transparent ITO layer is deposited on a glass substrate. This ITO functions as the anode to the blue OLED. The blue OLED is formed by the successive deposition of an HTL, a blue LEL, and then an ETL. A thin (~ 100 Å) and approximately 50% transparent Mg-Ag alloy is thermally evaporated onto the structure to serve as the cathode for both the blue and green OLEDs. To form the inverted green OLED, a green, fluorescent, organic thin-film is deposited. Next, an HTL is added, followed by the sputtering of ITO to form the shared anode for the green and red OLEDs. To form the red OLED, a third HTL is deposited. Then a red LEL is deposited followed by the deposition of a thick (~ 1500 Å) Mg-Ag electron-injecting cathode. To finish the structure, a layer of Ag is deposited to reduce oxidation of the Mg.[38] A structure of this nature can only be achieved with the use of organic materials; no such structure, constructed from numerous heterogeneous layers, could be fabricated using crystalline inorganic materials due to their strict lattice-matching requirements.

A useful variation of the SOLED structure can be formed by splitting the top ITO electrode (i.e., the electrode shared by the green and red OLEDs) into two separate electrodes. This can be easily achieved by depositing a transparent insulating oxide or organic layer following the ITO deposition. Then another layer of ITO can be deposited to form the anode of the red OLED. This structure is slightly more complex, but has several advantages. One significant advantage is the simplification of the driving circuit. The previous SOLED structure, with the shared ITO electrode, necessitates differential biasing of the red OLED and therefore requires a complex driving scheme. With the splitting of the electrode, each OLED can be addressed independently, and the driving circuit is similar to the one

used by the lateral subpixel scheme. Another advantage of this structure is the use of the thickness of the transparent insulating layer to tune the optical cavity length, thereby eliminating or reducing unwanted microcavity effects.[64] The final SOLED structure is three separate, stacked R, G, and B subpixels that can be addressed independently, providing one full-color pixel.

In the SOLED structure, some drawbacks are inevitable. Semitransparent electrodes for the middle subpixel introduce a loss of efficiency due to light absorption. Fortunately, several low-absorption metal-containing or metal-free electrodes, such as CuPc and BCP, have been found to reduce absorption and enhance the efficiency.[70] Additionally, these electrodes are able to reduce the microcavity effects. Another problem is color bleeding due to energy down-conversion of light emitted from the blue OLED upon passing through the red LEL. This problem can be minimized by the use of guest-host doped layers for the devices emitting at longer wavelengths.

To sum up all the subpixel techniques we have discussed, a review of the main advantages and disadvantages of each structure is presented in Table 5.3.

5.4 OLED Stability and Encapsulation for Displays

In this section, the detrimental impact of moisture and oxygen on OLED properties is addressed with a description of the formation, growth, and influence of dark spots. Then, several methods to encapsulate OLEDs are briefly summarized.

5.4.1 Impact of moisture and oxygen

Even though the good performance of OLEDs in inert gases has been demonstrated, the lifetime in air is very short and therefore inadequate for commercial applications. The short lifetime of an OLED is due to its exposure to water vapor and oxygen that are present in the air.[28, 68] A basic OLED is composed of a transparent electrode such as ITO, an EL layer, and a metal layer. The influences of air exposure on each layer are described in detail below.

The polymers used in the EL layer are usually very sensitive to photo-oxidation. This leads to an interruption of the polymer conjugation length by changing their chemical structures. A reduction of conjugation length and polymer bleaching will be the final result of this process. To verify this process experimentally, a Kr laser with the wavelength at 482 nm was used to irradiate PPV, which is typically used as the EL layer, and the transmission was measured as a function of time under three different conditions. According to the results, shown in Fig. 5.11, the increase of PPV's transmission with exposure time in air is more rapid than that occurring in water vapor and a vacuum. Hence, water vapor was able to cause photobleaching, e.g., an increase of polymer transmission; so was oxygen. Moreover, the influence of oxygen on the polymer degradation was stronger than that of water vapor.

Table 5.3 Summary of different subpixel structures used to achieve full-color displays.

Technique	Advantages	Disadvantages
Side-by-side RGB (shadow-mask method)	1. No power penalty 2. High quantum and power efficiency 3. Low fabrication cost	1. Low resolution 2. Limited display panel size
Filtering of white OLED by absorptive filters	1. High resolution 2. Easy fabrication 3. Can be transplanted from LCD technology	1. Low efficiency 2. High driving current 3. Short lifetime 4. High power consumption 5. Expensive color filters
Filtering of white OLED by dielectric multilayer structure	1. Enhanced output intensity 2. Slightly lower driving current	1. Complex fabrication 2. Small viewing angle
Down-conversion of blue light to red and green light	1. High resolution	1. Low contrast 2. High fabrication cost 3. Color bleeding
Color-tunable pixels	1. High resolution 2. Tunable spectrum	1. High operating voltage 2. Fast degradation 3. Complex drivers
Pyramid-shaped pixels	1. High resolution 2. Mask-free fabrication 3. Enhanced quantum efficiency	1. Pyramid-shaped substrates needed 2. Small viewing angle 3. Complicated electrical connections and addressing scheme
Stacked OLED (SOLED)	1. High resolution 2. High efficiency	1. Absorption by semitransparent electrode 2. Color bleeding 3. Microcavity effect 4. Complex drivers

The cathode in OLEDs is used to inject electrons into the EL layer. It should be made of a metal with a low work function. However, if it is exposed to water vapor or oxygen, it will very quickly form metal oxide due to its highly reactive nature. Instead of direct metal corrosion, water vapor and oxygen can also permeate through the cathode and form oxide at the interface between the metal and polymer layers. This was also verified by the measurement of x-ray photon-electron spectroscopy (XPS). The XPS spectrum is shown in Fig. 5.12. The oxide layer present at the metal interface polymer has negative effects on the device's performance since it modifies the barrier for electron injection into the EL layer. A higher resistance present at this interface will require a large current density or voltage value to produce light emission.

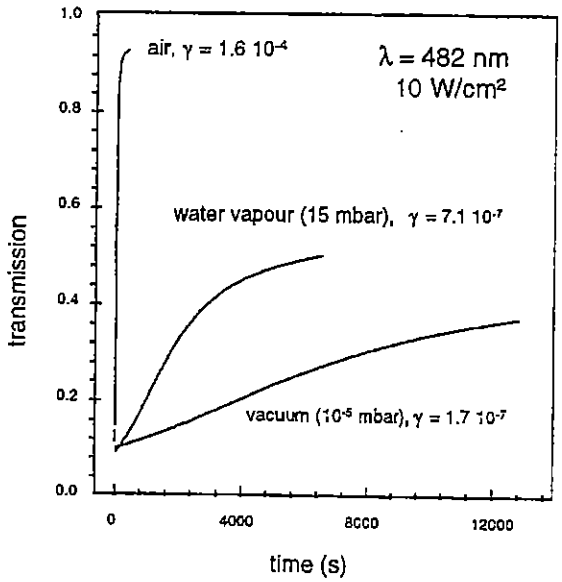

Figure 5.11 Evolution of PPV transmission under air, water vapor, and a vacuum with time exposure. Adapted from Ref. [28] with permission of Elsevier.

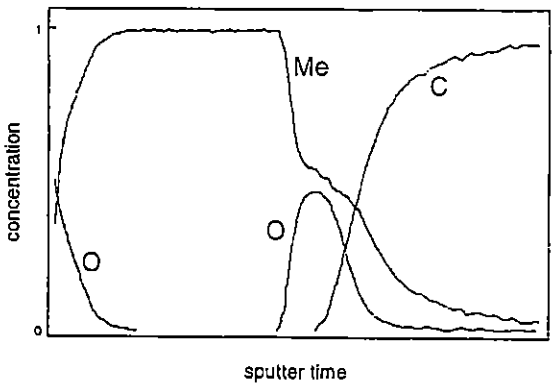

Figure 5.12 XPS spectrum of an OLED. Adapted from Ref. [28] with permission of Elsevier.

The anode in an OLED is used to extract electrons from (or inject holes into) the EL layer. Although there are papers[28, 29] reporting that a UV/ozone or oxygen plasma treatment of ITO can improve OLED performance considerably, the improvements are not stable. This treatment will increase oxygen concentration at the ITO surface. Since oxygen is electro-negative, it will form a negatively charged surface layer at the ITO/EL layer interface resulting in repulsion and depletion of electrons just beneath the surface of the ITO. This will induce band bending and a higher work function of the ITO that is responsible for a higher density of holes near the interface.

5.4.2 Influence of dark spots

Another fatal factor that can greatly reduce an OLED's lifetime is dark spot formation. There are at least two possible origins of dark spots. One is due to dust particles,[111, 117] and the other is due to high local-current flux.[66]

Dust is unavoidable in the OLED fabrication processes. Dust particles create a shadow effect during evaporation of the organic material and leave spaces inside the light-emitting material. If the dimension of the particles is larger than the thickness of the OLEDs, there is no doubt that the device will not emit light from this region. Moreover, water and oxygen can more easily penetrate into the devices through these large areas, because even if the dust particle size is smaller than the OLED thickness, they provide sufficient spaces for water and oxygen to permeate inside the film. Figure 5.13 shows the time evolution of dark spots. It should be noted that the size of dark spots increases with time but their number typically remains the same.

The high local-current density is another cause of dark spots. From the EL measurement it was concluded that bright spots will evolve into dark spots, which can be seen in Fig. 5.14. The bright spots probably come from a high local conductivity due to the reduced thickness of the EL layer, a thicker metal film, or better contacts. As soon as bright spots are formed, the local-current density becomes very high, which will cause a local increase in temperature due to large local joule heating. Unfortunately, the higher the temperature, the larger the polymer's conductivity, resulting in positive feedback. The high temperature can also trigger the interdiffusion of organic layers and/or contact metal inside the OLED layer, which will result in a low conductivity and the formation of dark spots. As time goes by, the size of the dark spots grows. The stages of this effect are shown in Fig. 5.15.

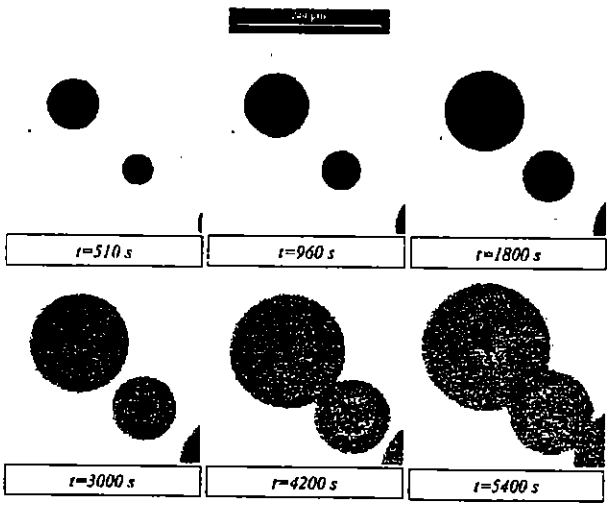

Figure 5.13 Time evolution of dark spot formation. Reprinted from Ref. [111] with permission of the American Institute of Physics.

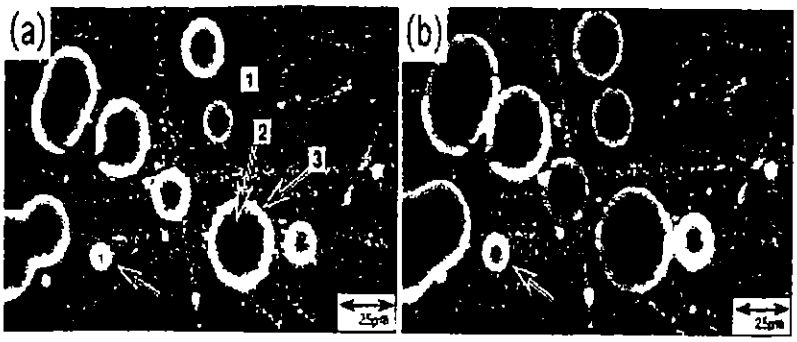

Figure 5.14 EL spectra showing dark and bright spots at different stages of formation. Reprinted from Ref. [66] with permission of the American Institute of Physics.

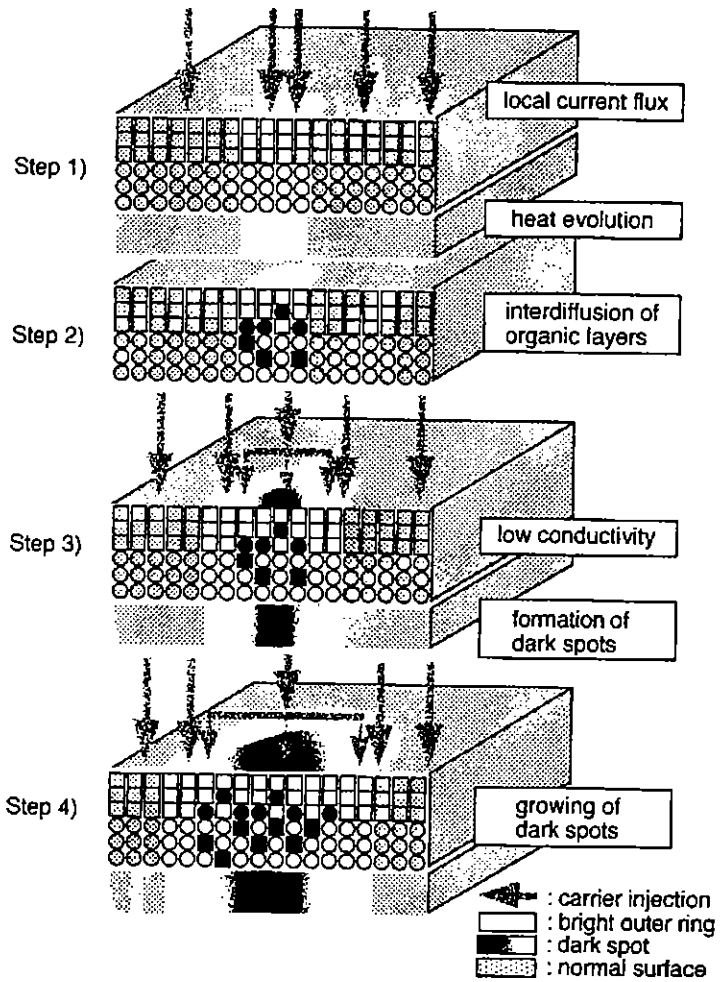

Figure 5.15 A propagation mechanism of dark spots. Reprinted from Ref. [66] with permission of the American Institute of Physics.

These dark spots are related more to the nonuniform OLED structure than to the influence of vapor and oxygen.

5.4.3 Encapsulation methods

To solve the problem of OLED lifetime, several methods have been proposed to encapsulate and seal OLEDs from humidity and oxygen. The simplest way is to use glass as a top cap with a nitrogen-filled chamber.[37] A schematic of the structure is shown in Fig. 5.16. This configuration uses epoxy, a widely used encapsulant in electronic packaging. In addition, a-SiN_x is deposited to reduce the permeability of humidity and oxygen from the sides.

Another method is to encapsulate OLEDs by sealing canisters with a UV adhesive such as epoxy resin under a nitrogen atmosphere,[103] which is a common method to seal semiconductor LEDs. In addition, a plasma-enhanced chemical vapor deposition (PECVD) silicon nitride film (a-SiN_x) is always deposited for passivation to provide low film stress and a good barrier against humidity and oxygen, with BaO added as a resistive absorbent.

The third approach utilizes a stack of alternating polymer and transparent dielectric layers to protect OLEDs from the permeation of water and oxygen through the substrate.[73] Preferably, the dielectric layer is fabricated from silicon monoxide (SiO), silicon oxide (SiOx), silicon dioxide (SiO_2), or silicon nitride (Si_3N_4). As for the polymer layer, it can be chosen from a group of robust polymers such as fluorinated polymers, parylenes, and cyclotenes. On top of the OLEDs, the hermetic sealing consists of several layers including a buffer layer, followed by a thermal coefficient matching layer, and then an inorganic layer with low permeability. The buffer layer may be either an organic polymer, such as a parylene with

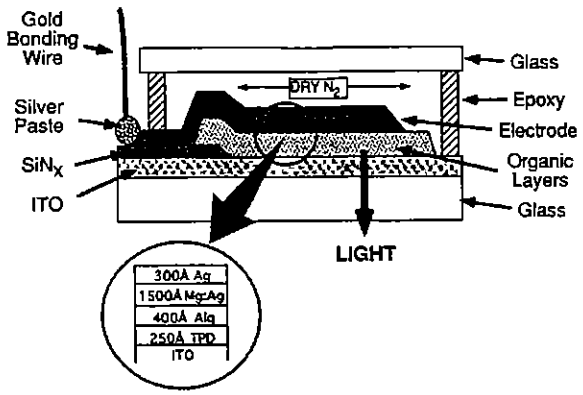

Figure 5.16 Schematic cross-section of an encapsulated, nitrogen-filled OLED with a detailed view of the thin-film layers. Reprinted from Ref. [37] with permission of the American Institute of Physics.

a low thermal expansion coefficient, or an organometallic complex such as Alq_3. For example, SiO_2 can be used as the thermal coefficient matching layer while Si_3N_4 functions as the inorganic outermost layer. A schematic side view is shown in Fig. 5.17. Outside the plurality of layers, epoxy and a thin metal foil can be added to strengthen its effectiveness against water and oxygen permeation.

The fourth approach[141] is similar to the first one. It uses glass, quartz, or thin silicon as a cap to provide cost and weight advantages. The perimetric seal is comprised of an electrically insulating layer, adhesion layers, and sealing layers, which is depicted in Fig. 5.18. Usually indium, tin, or gold is used for the sealing layers and titanium is used as the adhesion layers. The sealing process is accomplished by using pressure and a heating element.

The last method does not use epoxy coating, which tends to degrade the device property due to the infiltration of the solvent into the EL layer. In this scheme, a dielectric layer is coated on top of metallic cathodes and a metal film is added above the dielectric layer.[91] The basic structure is shown in Fig. 5.19. Although the polymers used to protect devices in some approaches have excellent electrical resistivity, the high breakdown strength and transparency, and the ability to avoid permeation of water, are not good enough. Furthermore, some metal films

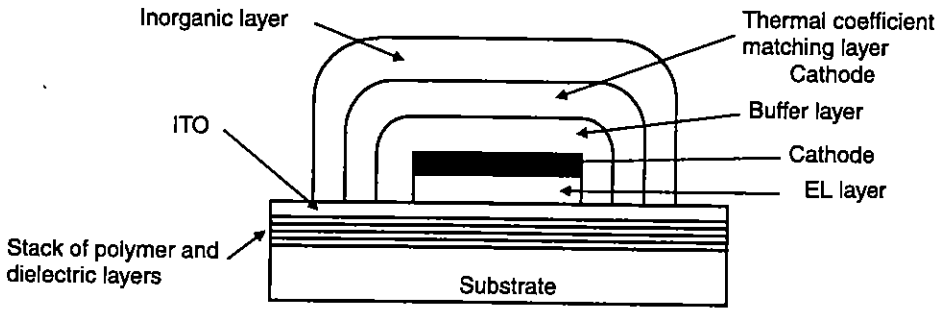

Figure 5.17 Cross-section side view of an encapsulated OLED.

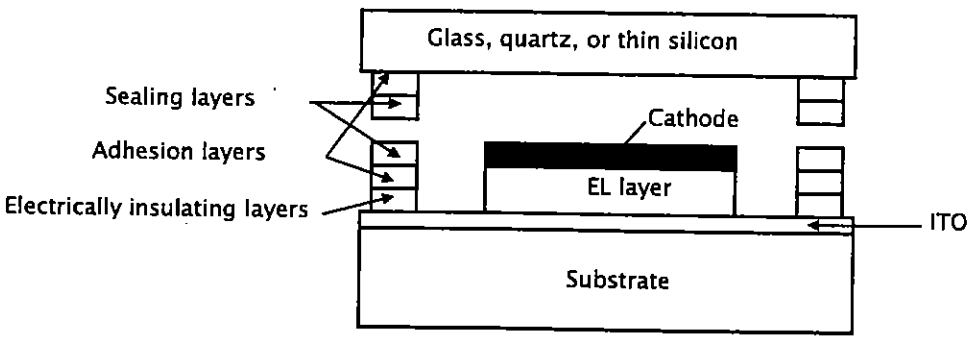

Figure 5.18 Side view of an encapsulated OLED.

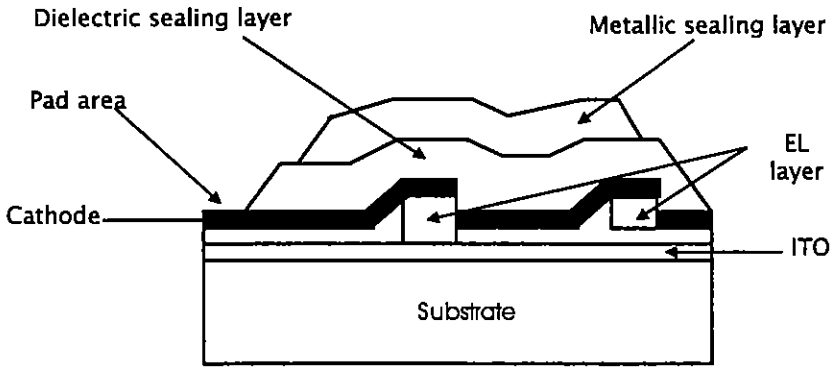

Figure 5.19 Cross section of an encapsulated OLED. Adapted from Ref. [170] with permission of Elsevier.

are also used to seal OLEDs, but they should be relatively thick to avoid pinholes, which leads to poor light transmission. In this method, only two thin layers are needed. The dielectric layer is preferably composed of a SiC film with a thickness of 500 nm, deposited by PECVD from trimethylsilane. Alternatively, diamond-like carbon (DLC), SiO, SiO_2, Si_3N_4, or silicon oxynitride (SiO_xN_y) can also be used. The PECVD-deposited SiC provides high dielectric strength, good film adhesion, a low pinhole density, and impermeability. Additionally, this dielectric layer may consist of a combination of several materials—for example, SiO_2 and SiC, DLC and SiC, or Si_3N_4 and SiO_2. As for the metal film, it is better to use sputtering deposition. Sometimes, a combination of PECVD and an electron beam or sputtering deposition achieves the lowest pinhole density. The function of the metal film is to reduce the device's susceptibility to cracking under stress, and to preseal the pinholes. The device is then baked, preferably in purified air or a dry nitrogen-oxygen atmosphere. The metals will react with oxygen or moisture to adsorb gases and seal off pinholes inside the layer. This beneficial property removes pathways for oxygen and moisture. When patterning the dielectric and metal films, a shadow mask may be employed where external connections are required.

5.5 Display Addressing and Driving Circuit

In this section, we describe several addressing schemes and driving circuits that have been used to control OLED flat-panel devices. We assume that the data timing and multiplexing to the appropriate column electrode has been taken care of so we can focus on the individual pixel driving mechanisms. Two main categories of display driving schemes exist: direct addressing and matrix addressing. We will begin with a short description of direct addressing and then move to the explanation of two different types of matrix addressing.

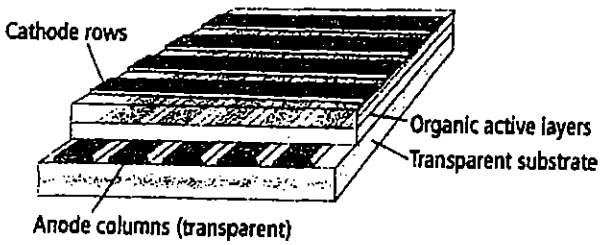

Figure 5.20 Matrix addressing of an OLED. Adapted from Ref. [64] with permission of the IEEE.

In direct addressing, each pixel is connected to an individual driver. This scheme is most efficiently used in alphanumeric displays, such as the common seven-segment display, and discrete indicator displays.[70] This type of addressing is not applicable to video-rate FPD technology. However, direct addressing is useful where the display is relatively simple and low-information contents are displayed, but the pixel is in the form of a complex pattern that is simply turned on and off.

In matrix addressing, the pixels are arranged into a two-dimensional array of rows and columns. Each pixel is then connected to one row lead and one column lead as shown in Fig. 5.20.[64] The matrix addressing scheme in which active electronic devices such as TFTs are used to enhance the display characteristics is termed active-matrix (AM) addressing. A much simpler addressing scheme in which no extra active electronic devices are used is termed passive-matrix (PM) addressing. With the use of matrix addressing schemes, arrays of OLEDs can be used as high information content and video-rate FPDs.[70]

5.5.1 PM-addressing method

In a PM-addressed display, the organic light emitter is connected to a row electrode and an orthogonal, electrically isolated, column electrode. An equivalent circuit of this scheme is shown in Fig. 5.21. The diode represents the OLED sandwiched at the intersection of the row and column electrodes. The fabrication process is relatively simple. First, the row electrode (anode) material, usually ITO, is deposited onto the transparent glass substrate and then patterned using photolithography to achieve fine features. Next, the organic layers are deposited in one of the schemes discussed above to create R, G, and B subpixels. Finally, the conducting column electrode material (metal alloy cathode) is deposited using a shadow mask to avoid the exposure of the organic layers to moisture during the etching of the electrode lines. The mechanical shadow mask method does not give nearly the resolution that is provided by photolithography.

The operation principle of a PM-addressed display is straightforward. Each row electrode (anode) is connected to an electronic switch and each column elec-

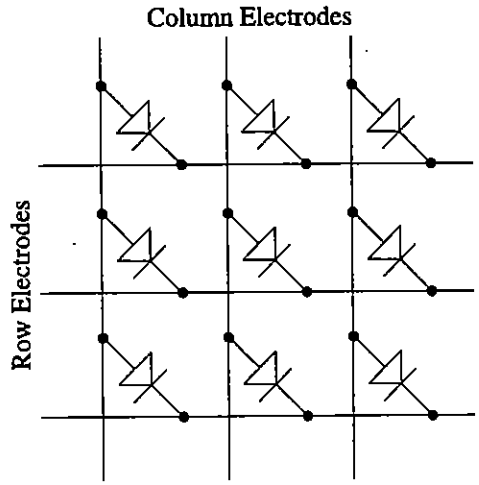

Figure 5.21 Equivalent circuit of the PM-addressing scheme.

trode (cathode) is connected to a current source. Since light emission from the pixel is dependent on the current passing through the OLED, current sources must be used to effectively realize different gray levels.[70] The row electrodes are scanned in succession (row-by-row) at a frame rate that is greater than 60 frames per second. The data signals, which are electric current signals, are applied to the column electrodes with the proper timing, thereby successively turning the pixels on and off.

Several disadvantages exist with the PM-addressing scheme. One problem is caused when one of the pixels in the display malfunctions, i.e., the pixel is shorted or leaky. This can cause other pixels near the "bad" pixel to be unintentionally addressed. This event is one of many forms of crosstalk and disrupts the normal operation of the display. Another problem is due to an inherent characteristic of the OLED. Consider a display with M rows. With the row-by-row scanning scheme, each of the OLEDs is powered on for a maximum of $1/M$ of the frame period. Since OLEDs have no memory effect, they will be off unless they are addressed and driven by the external power source. In order to achieve the required average display panel brightness of, for example, 100 cd/m^2 in a frame period, each OLED must be driven at a brightness of $M \times 100$ cd/m^2. Large currents are needed to achieve the required brightness when M is large, thereby causing accelerated degradation of the OLED. Besides, the OLED emission efficiency decreases at a high current level, which also causes fast degradation of the OLED. Another disadvantage arises from the number and size of electrode lines used in the display. If M is large, appreciable and unwanted voltage drops may occur across the electrodes, causing the pixels to display incorrect information. This limits the total number of rows to approximately 500, which is far below the number required for a high-information content and a high-resolution FPD.[70] AM-addressing schemes can be used to alleviate these problems.

5.5.2 AM-addressing method

As stated above, matrix addressing schemes that utilize active electronic components at each pixel site are termed active matrix (AM). These active switching elements are usually TFTs with poly-Si, a-Si:H, or an organic semiconducting small molecule or polymer film (OTFTs) used as the channel region material. Due to the lack of memory effect in OLEDs, at least two TFTs per pixel (or subpixel for full-color displays) are needed for an effective AM-addressing circuit (see Fig. 5.22).

The circuit has one control line (V_{select}), one data line (V_{data}), and power/ground lines. The external driving circuits consist of gate and source drivers. The V_{select} line is connected to the gate drivers, and the source drivers supply data to the source of T1 in each pixel circuit. The V_{select} line is set to high for data to be written to the pixel. Here, the signal V_{data} charges the storage capacitor to the desired voltage (C_{st}). The voltage on the storage capacitor remains constant even after V_{select} switches to low (–5 V) except for the initial drop due to the parasitic capacitance of T1 when T1 turns off. The current flowing through the OLED (I_{OLED}) is controlled by the drive transistor, T2. When T2 is biased in saturation, the current I_{OLED} is

$$I_{OLED} = \frac{\mu CW}{2L}(V_{GS} - V_{th})^2, \tag{5.2}$$

where μ, C, W, and L are the channel mobility, the channel capacitance, the channel width, and the channel length of the transistor, respectively; V_{GS} is the gate to the source voltage; and V_{th} is the threshold voltage of the TFT.

In the voltage driving configuration, a slight threshold voltage variation in the OLED could be the result of the long-term operation or the process nonuniformity. This variation will charge the current flowing through the OLED since the V_{GS} of T2 is dependent on the drop across the OLED. When a current driving circuit is used and V_{DD} is large (T2 in deep saturation), the variation in threshold

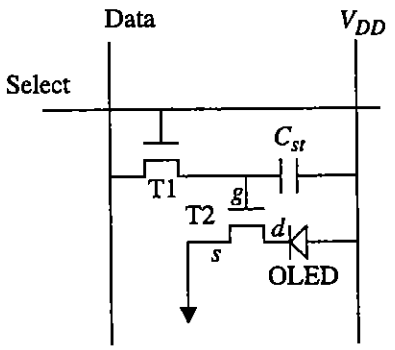

Figure 5.22 AM-addressing scheme using two TFTs per pixel.

voltage of the OLED will not affect the current because the V_{GS} of T2 remains unchanged. Therefore, a constant current configuration circuit is preferred for an AMOLED. This type of OLED addressing will be discussed in more detail below.

5.6 TFT Technology for AM Displays

The TFT is an important switching and driving element in the AM-addressing scheme. The TFT is also an essential element for achieving high-resolution and integrated-driver AM addressing. The TFTs can be made using a-Si:H, poly-Si, or organic semiconductors as the active region of the TFT. Although we will not go into the details of the electrical properties of these devices, we will present two requirements that must be fulfilled in order for the TFTs to be effective in the pixel electrode driving circuits that are discussed below. For the details, the reader is referred to Ref. [70]. In order to fully charge the storage capacitor of the pixel circuit, the ON-current must be sufficiently large. Also, in order to maintain the bias on the gate of T2, the OFF-current must be sufficiently small. This leads to the first TFT requirement, which is the ON-current (I_{on}) to OFF-current (I_{off}) ratio

$$\frac{I_{on}}{I_{off}} \geq 2SMN_g \,. \tag{5.3}$$

Here, S is an engineering safety margin, M is the number of rows, and N_g is the number of gray levels. If we take $M = 1024$, $N_g = 256$, and $S = 3$, then $I_{on}/I_{off} \geq 8 \times 10^5$. This ratio is easily achieved with the use of a-Si:H TFTs with $I_{on}/I_{off} \sim 10^7$, poly-Si TFTs with $I_{on}/I_{off} \sim 10^6$, or with organic TFTs with $I_{on}/I_{off} \sim 10^8$ (Ref. [70]).

The second requirement is an estimation of the field-effect mobility, μ_{FET}, needed to allow the complete charging of the pixel electrode storage capacitor in the allotted time frame. To make this estimate, the following equation has been developed:

$$\mu_{FET}\frac{W_2}{L_2} \geq \frac{5MC_{pix}}{T_f C_{OX}(V_{GS2} - V_{th})}, \tag{5.4}$$

where μ_{FET} is the field effect mobility, W_2 is the width of T_2, L_2 is the length of T2, M is the total number of rows, C_{pix} is the total pixel capacitance, T_f is the frame time, C_{OX} is the insulator layer capacitance, V_{GS2} is the gate to the source voltage of T2, and V_{th} is the threshold voltage of the TFT. A simple calculation with judicious values gives $\mu_{FET}\, W_2/L_2 \geq 3$ cm^2/V$_s$. Again, this can be accomplished with a-Si:H, poly-Si, and organic TFTs that have reasonable W/L ratios.[70] In order to achieve a pixel brightness of 100 cd/m^2 from a sufficient pixel area, a current of approximately 10^{-7} A is required.

The a-Si:H and poly-Si based TFTs can provide the required ON/OFF current ratio and have carrier mobilities that allow fast switching speeds and charging of the pixel elements. In addition, the TFT needs to have sharp subthreshold slope and must be electrically stable over time. In general, the organic TFTs have insufficient subthreshold slope, and therefore have a high turn-on voltage (tens of volts). Also, they are not very stable electrically. Therefore, the organic TFTs are currently not a practical choice for AMOLEDs. Table 5.4 presents a comparison of typical values of certain parameters for a-Si:H and poly-Si TFTs. It shows that a-Si:H TFTs are capable of supplying the required current, and are therefore capable of driving OLED-based displays. Next, we discuss the technology and fabrication processes used to fabricate a-Si:H and poly-Si TFT AM arrays.

Table 5.4 Comparison of a-Si:H and poly-Si TFT properties.

Property	a-Si:H TFT	poly-Si TFT
Typical mobility ($cm^2/V{\cdot}s$)	0.6–1.0	50–100
TFT W/L ratio	10:1	10:1
Maximum current (A)	2.5×10^{-5}	2.1×10^{-3}
Maximum OLED luminance (cd/m^2)	5,000	$>4 \times 10^5$

5.6.1 a-Si:H TFT technology

The fabrication steps of a-Si:H TFTs for a four-TFT AM pixel electrode circuit was described by He et al.[77] The fabrication of this circuit is similar to that of a conventional inverted-staggered, back channel-etched a-Si:H TFT and is shown in Fig. 5.23. The first step is the deposition, by sputtering, of 1000 Å of chromium onto a Corning 1737 glass substrate. This layer is then patterned to form the TFT gate electrodes and the bottom electrode of the storage capacitor (a). Next, a 3000-Å layer of a-SiN_x:H, a 2000-Å layer of undoped a-Si:H, and a 500-Å layer of n+ a-Si:H are deposited, respectively, using PECVD (b). The active area of the TFT (a-Si:H) is then defined (c) and gate vias opened (d). Next, a 2000 Å-thick layer of molybdenum is deposited by sputtering and patterned to form the source and drain electrodes of the TFTs and the top electrode of the storage capacitor (e). The TFT is back channel-etched using reactive ion etching (RIE) (e). A 3000 Å-thick layer of a-SiN_x:H is deposited as a passivation layer and vias are opened (f). Finally, the electrode material (ITO) is sputtered, annealed, and etched (g).[77] The OLED structure is fabricated on the top of the ITO electrode. In this configuration the light is emitted through glass substrate.

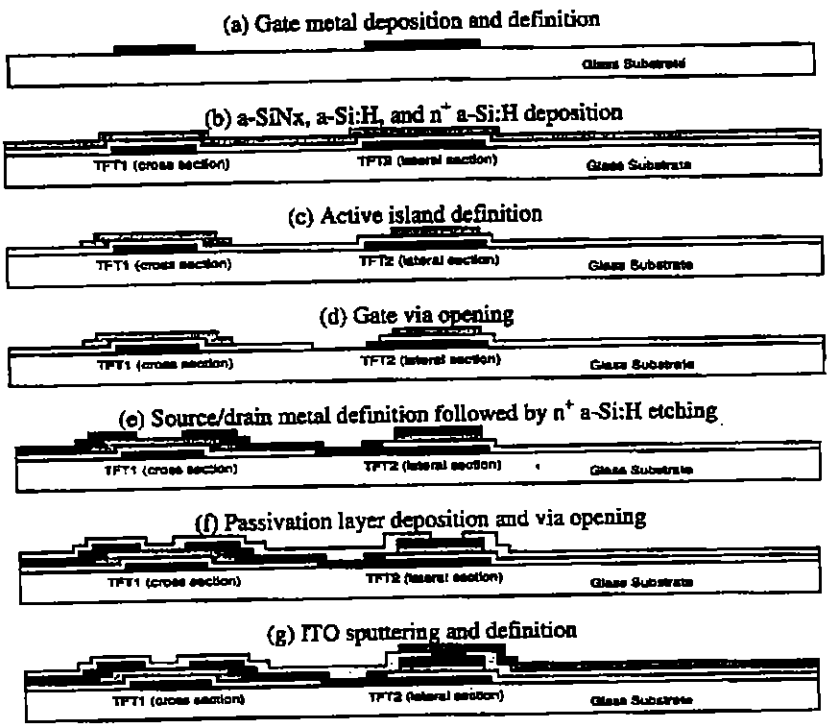

Figure 5.23 Fabrication process for an a-Si:H-based TFT AM pixel.

5.6.2 Poly-Si TFT Technology

Both high-temperature (HT, above 600°C) and low-temperature (LT, below 600°C) poly-Si TFTs are capable of driving high-resolution AMOLEDs. However, only the LT poly-Si TFTs have the capability to be fabricated on large transparent substrates. Therefore, we will describe one of the many LT poly-Si TFT technology and fabrication processes. The cross-sectional structure of the poly-Si TFT AM pixel is shown in Fig. 5.24.[100]

First, a 100-nm amorphous silicon film is deposited using low-pressure chemical vapor deposition (LPCVD). The a-Si:H film is then crystallized by laser annealing. In this approach, the film is irradiated multiple times by a KrF excimer laser to form a poly-crystalline film. The film is then etched to form a poly-Si island. Next, a gate insulator is formed using plasma-enhanced chemical vapor deposition (PECVD) of SiO_2 or a-SiN_x. A poly-Si gate layer is deposited and etched. Next, phosphorous (boron) is implanted to form a self-aligned n-channel (p-channel) TFT. To finish the TFT, a metal (Al) layer is sputtered and etched to form bus lines and a gate, and source and drain connections. The TFT is passivated with an insulating layer, and vias are opened in this layer to allow the contact to the ITO electrode. ITO is deposited and etched to form the anode of the

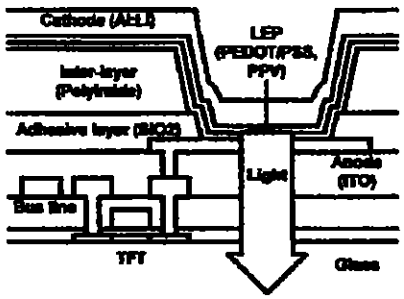

Figure 5.24 Cross section of a poly-Si TFT AM pixel. Reprinted from Ref. [100] with permission of the IEEE.

OLED.[100] Again, the OLED is fabricated over the ITO electrode. In this configuration the light is emitted through glass substrate.

In this pixel circuit, p-channel poly-Si TFTs are used due to good electrical device reliability. In general, it is accepted that the p-channel device is much more electrically stable than the n-channel device.

5.6.3 Pixel electrode circuits

Unlike typical AMLCDs where one TFT is used as a switch, in AMOLEDs at least two TFTs are needed, as shown in Figs. 5.22 and 5.25. One TFT (T1) is used as a switching device and the other TFT (T2) is used as a current-driving device, because a continuous current flow through the pixel_OLED is required during a frame time for a continuous pixel light-emission. As indicated above, the TFTs can be fabricated from a-Si:H or poly-Si thin films. So far, the poly-Si TFT technology has been used most frequently in AMOLEDs because the poly-Si TFTs show better electrical performance (high field-effect mobility) and higher electrical stabil-

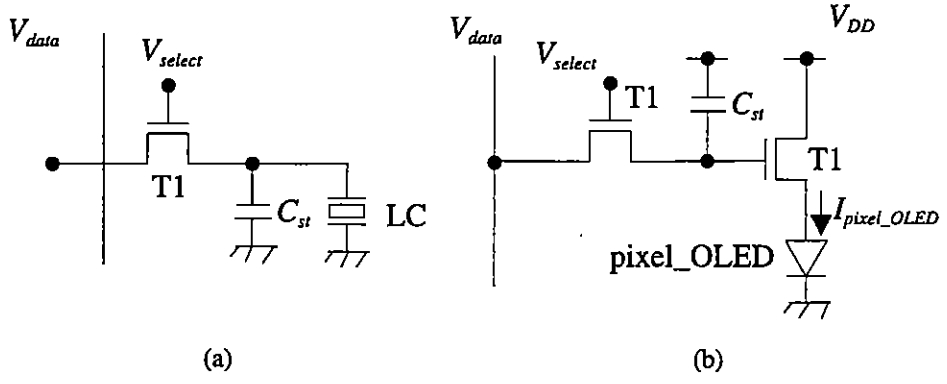

Figure 5.25 An example of the pixel electrode circuit for (a) an AMLCD, and (b) an AMOLED.

Table 5.5 Comparison of LT poly-Si and a-Si:H TFT properties.

Property	LT poly-Si TFT	a-Si:H TFT
Threshold voltage (V)	3–5	~2
Field-effect mobility (cm^2/Vs)	50–120	~1
Off current	$10^{-11} - 10^{-9}$ A	$10^{-13} - 10^{-12}$ A
Maximum process temperature (°C)	550–600	150–300
Driver integration	Yes	Possible
Threshold voltage stability	Good	OK
Mobility and threshold voltage variation over large area	OK	Very good
Manufacturability	Maturing	Very mature
Cost	High	Low
Plastic compatibility	Developing	Good

ity (lower threshold voltage shift) in comparison with a-Si:H TFTs. Table 5.5 shows the electrical performance, advantages, and disadvantages of the LT poly-Si and a-Si:H TFTs for AMOLEDs.[85, 100, 118, 127]

The advantages of LT poly-Si TFTs are as follows:

- A low driving voltage is needed to produce a given current flow through the OLED due to the high TFT field-effect mobility.
- The peripheral driver circuit can be integrated on the display substrates.
- The TFT threshold voltage is stable during display operation.

The disadvantages of LT poly-Si TFTs are as follows:

- The off current is rather high, which can cause an undesirable charge leakage problem through the switching TFT when the pixel is deselected.
- The TFT threshold voltage and field-effect mobility are not uniform over large areas, since laser crystallization is used to produce poly-Si film.
- The manufacturing techniques are expensive and not yet mature.
- The rather high-temperature process may not be compatible with plastic substrates.

The advantages and disadvantages of poly-Si TFTs can, conversely, be the disadvantages and advantages of a-Si:H TFTs. For example, the low driving-current capacity of a-Si:H TFTs, due to their rather low field-effect mobility, has been a significant issue in AMOLEDs that are based on a-Si:H TFT technology. However, dramatic progress made recently in the luminous efficiency of light-emitting

organic[72] or polymeric[27, 122] materials has rendered a-Si:H TFT technology as a competing technology in AMOLEDs. Several AMOLED prototypes based on a-Si:H TFT technology have been described recently in the literature.[85, 99, 110]

Although the prototypes of poly-Si and a-Si:H TFT AMOLEDs have already been demonstrated, the device parameter variations of the OLEDs and TFTs are still critical issues for the operation stability of AMOLEDs. The OLED threshold voltage may vary from pixel to pixel after fabrication, then increase slowly at 0.1–1 mV/hour[146] during display operation. The field-effect mobility of both poly-Si and a-Si:H TFTs may vary from pixel to pixel due to either process variations or device aging effects.[85, 146] These effects must be compensated for in an AMOLED in order to obtain a uniform light emission and stable operation of the display. This compensation can be achieved by selecting an appropriate AMOLED pixel electrode circuit configuration based on either voltage-driven[49, 99, 146, 151] or current-driven[50, 56, 84, 132, 147] schemes. In the voltage- and current-driven pixel electrode circuits, voltage and current, respectively, are used as data signals.

Figure 5.25(b) shows a simple voltage-driven pixel electrode circuit with two n-type TFTs. As previously noted, T1 and T2 act as a switching TFT and a driving TFT, respectively. T1 operates in the linear regime and T2 in either the linear or saturation regimes. When V_{select} is high (select time), T1 is on. A data voltage is written onto the storage capacitor (C_{st}) through T1, and the corresponding current (I_{pixel_OLED}) flows from the voltage data-drive, V_{DD}, through T2 to pixel_OLED. Then the pixel will emit light. When V_{select} is low (deselect time), T1 is off and the stored voltage (C_{st}) determines the amount of the current flow through pixel_OLED. Therefore, if there is no change in the stored voltage, the same amount of current flows from V_{DD} through T2 to *pixel_OLED*, producing a continuous pixel light-emission with the same brightness. However, in this simple voltage-driven pixel electrode circuit, I_{pixel_OLED} can vary because the data voltage is a summation of V_{GS_T2} and voltage across the pixel_OLED. This will lead to nonuniform display light-emission if there are any changes in the turn-on voltage of the pixel_OLED and threshold voltage of the TFTs at a given data voltage.[146] Therefore, simple voltage-driven pixel electrode circuits cannot be used in AMOLEDs to produce a uniform brightness level across the whole display.

Based on the simple voltage-driven pixel electrode circuit, researchers at Seiko-Epson Corporation and Cambridge Display Technology[151] reported the area ratio gray scale (ARGS) method to achieve uniform light emission of an AMOLED. They used the poly-Si TFT technology as shown in Fig. 5.26. In the ARGS method, each pixel consists of nine same-dimension subpixels with one n-type (T1) TFT and one p-type (T2) TFT; T1 operates as a switching device and T2 operates as a switch-like driving device. Instead of changing the T2 driving current to produce gray scales as in a simple voltage-driven pixel electrode circuit, in the ARGS method the gray scale is obtained by selecting the number of light-emitting subpixels; thus, 10 gray scales can be achieved with a nine-subpixel structure. The subpixel operates like a binary mode by applying two separate V_{data} values that are either high or low enough to fully turn on and off T2, respectively, no mat-

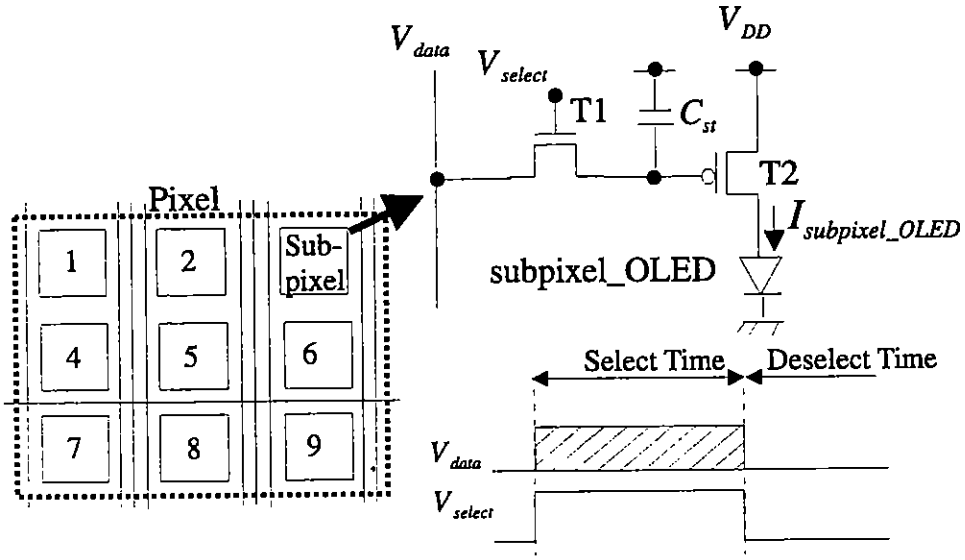

Figure 5.26 Area ratio gray scale (ARGS) method based on a simple voltage-driven AMOLED pixel electrode circuit proposed by Shimoda et al.[150, 151]

ter what change occurs in the T2 threshold voltage. In addition, V_{DD} determines the current level through the subpixel_OLED. Therefore, the T2 threshold voltage shift will not change the current flow through the subpixel_OLED. However, the ARGS method is limited because the number of subpixels determines the possible number of gray scales. To increase the number of gray scales, the ARGS method can be combined with the time ratio gray scale (TRGS) method, which requires a complicated subframe driving scheme and an additional erase scan TFT in each subpixel.[150]

The first voltage-driven pixel electrode circuit with the threshold voltage compensation was reported by Dawson et al.[49] Their circuit consists of four p-type poly-Si TFTs, one selection (V_{select}), and two control lines (AZ and AZB), as shown in Fig. 5.27(a). T1, T3, and T4 are switching TFTs, and T2 is a driving TFT. When V_{select} is low (select time), T1 is on. The select time consists of five subperiods. During periods 1 and 2, $|V_{GS\_T2}|$ is larger than the magnitude of the T2 threshold voltage, $|V_{th\_T2}|$, which is stored across the storage capacitor (C_{st2}). Then, during periods 3 and 4, T2 conducts until $|V_{GS\_T2}|$ is equal to $|V_{th\_T2}|$, storing the V_{th_T2} across C_{st2}. When V_{data} is reduced by ΔV_{data} (period 5), $|V_{GS\_T2}| = |V_{th\_T2}| + |\Delta V_{GS\_T2}|$, $|\Delta V_{GS\_T2}| = (|\Delta V_{data}| \times C_{st1})/(C_{st1} + C_{st2} + C_{G\_T2})$, where C_{G_T2} is the total gate parasitic capacitance of T2. When V_{select} is high (deselect time), T1 is off. The stored V_{GS_T2} is maintained during periods 6 and 7 until T4 is on. Finally, $I_{pixel\_OLED} \propto (\Delta V_{GS\_T2})^2 \propto (\Delta V_{data})^2$ during period 8, which indicates that the current flow through the pixel_OLED depends on ΔV_{data}, not V_{data} or V_{th_T2}. However, this pixel electrode circuit has two control lines, which can make the pixel electrode circuit configuration rather complicated and may cause threshold voltage settling and data voltage writing problems within a row select time.[146]

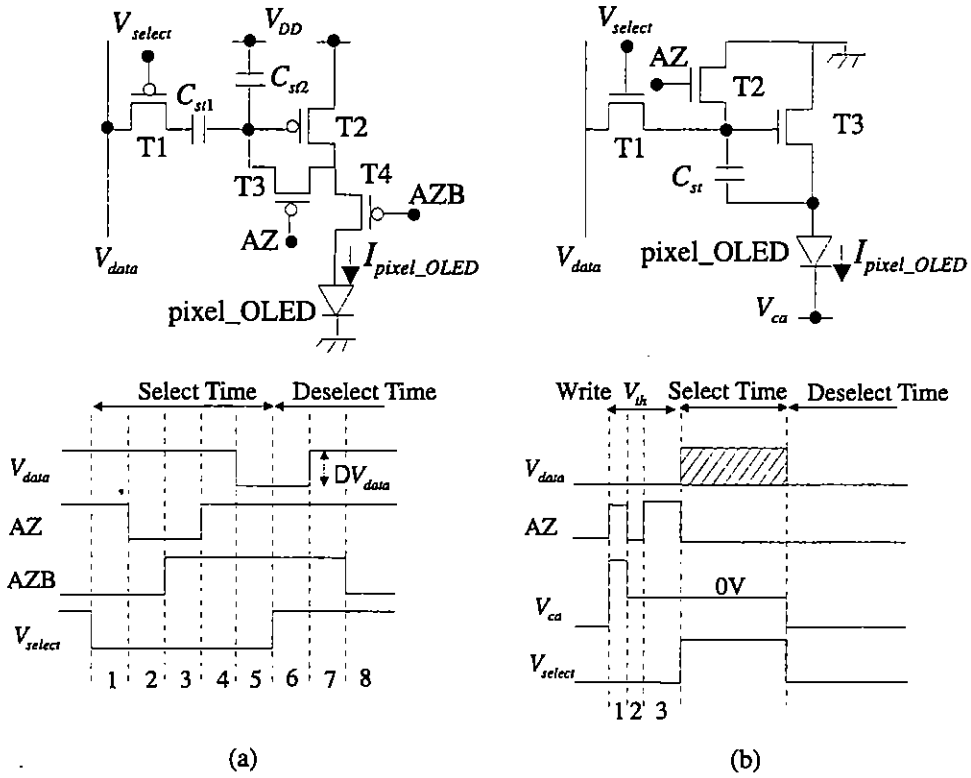

Figure 5.27 Two types of voltage-driven pixel electrode circuits with threshold voltage compensation. The circuit in (a) was proposed by Dawson et al.[49] and the circuit in (b) by Sanford et al.[146]

Another voltage-driven pixel electrode circuit has been reported by Stanford et al.[146] Their circuit consists of three n-type TFTs, one select (V_{select}), one control line (AZ), and one programmable cathode line (V_{ca}), as shown in Fig. 5.27(b). T1 and T2 are switching TFTs, and T3 is a driving TFT. This pixel electrode circuit can compensate for the TFT threshold voltage with the proper signals and timing. Writing the threshold voltage (periods 1 to 3 with V_{select} on low and T1 off) involves three steps. During period 1, while the cathode voltage V_{ca} is negative, the AZ input is high for a short amount of time. This establishes a capacitor voltage that is larger than the T3 threshold voltage. During period 2, V_{ca} is brought to positive voltage and the AZ input is low. T3 conducts, resulting in a negative voltage drop across the pixel_OLED. During period 3, V_{ca} is set at 0 V and the AZ input is set high. T3 conducts until a voltage approximately equal to the T3 threshold voltage is established across the storage capacitor. After this initial threshold voltage establishment, V_{select} is high and T1 is on, and then data voltage is written into the pixel circuit (select time) while V_{ca} is at 0 V and the AZ input is low. The voltage across the storage capacitor will be $V_{data} + V_{th\_T3}$. After data voltage has been written to all the rows in the display, V_{select} is set low and T1 is off (deselect time), and

V_{ca} is brought to a negative voltage. T3 will provide a current flow through the pixel_OLED, which is independent of V_{th_T3} and proportional to $(V_{data})^2$. In this pixel electrode circuit, the pixel_OLED emits the light only after the data voltage writing is finished.

The voltage-driven pixel electrode circuit can successfully compensate for the TFT threshold voltage variation. The operator can also compensate for the pixel_OLED threshold voltage shift by operating the driving TFT in the saturation regime, in which the current flow through the driving TFT (and thus through the pixel_OLED) depends on the V_{GS}, not the V_{DS} (voltage data-source), of the driving TFT. Therefore, although any voltage shift occurs in the pixel_OLED, changing the V_{DS} of the driving TFT will automatically compensate for it, and the current through the pixel_OLED will not change much. However, these voltage-driven driving schemes are limited to TFT threshold voltage compensation and are not adequate to compensate for the TFT field-effect mobility variations.

Several current-driven pixel electrode circuits[50, 56, 84, 132, 147] have been reported to fully compensate for TFT threshold voltage and field-effect mobility variations. In addition, since OLED brightness is directly related to the current flow through the device, the current-driven AM driving method has the benefit of producing a uniform display luminance by delivering current directly onto each pixel.

Dawson et al.[50] reported a current-programmed OLED pixel that consists of four poly-Si p-type TFTs, as shown in Fig. 5.28(a). T1, T3, and T4 are switching TFTs, and T2 is a driving TFT. In this pixel electrode circuit, the data current is written directly onto the pixel, and the corresponding charge will be stored across the storage capacitor. When V_{select} is low and the VGP (the voltage across the fourth transistor) is high (select time), T1 and T3 are on. Then current is provided by I_{data} through T3 and T2 to pixel_OLED, and the pixel_OLED emits light. A specific T2 gate-to-source voltage corresponding to the data current is simultaneously set across the storage capacitor. When V_{select} is high and VGP is low (deselect time), current is provided from V_{DD} through T4 and T2 to pixel_OLED, and pixel_OLED emits light. Since the stored V_{GS_T2} determines the current level during deselect time, the same amount of current flow is guaranteed through the pixel_OLED during the total time frame if T2 operates in the saturation regime.

Toshiba and Matsushita[132] reported a similar current-programmed pixel electrode circuit, as shown in Fig. 5.28(b), which they called a current-copy pixel (CCP). The CCP consists of four p-type poly-Si TFTs. T1, T3, and T4 are switching devices, and T2 is a driving device. When $V_{select1}$ is low and $V_{select2}$ is high (select time), T1 and T3 are on and T4 is off. Current flows from V_{DD} through T2 and T3 to the current source. The storage capacitor is charged during select time. When $V_{select1}$ is high and $V_{select2}$ is low (deselect time), T1 and T3 are off and T4 is on. Current flows from V_{DD} through T2 and T4 to the pixel_OLED. The amount of current during deselect time is determined by the stored voltage across the storage capacitor; thus, the same amount of current flow is again guaranteed if T2 operates in the saturation regime and there is no stored charge variation. The pixel_OLED emits light only during deselect time.

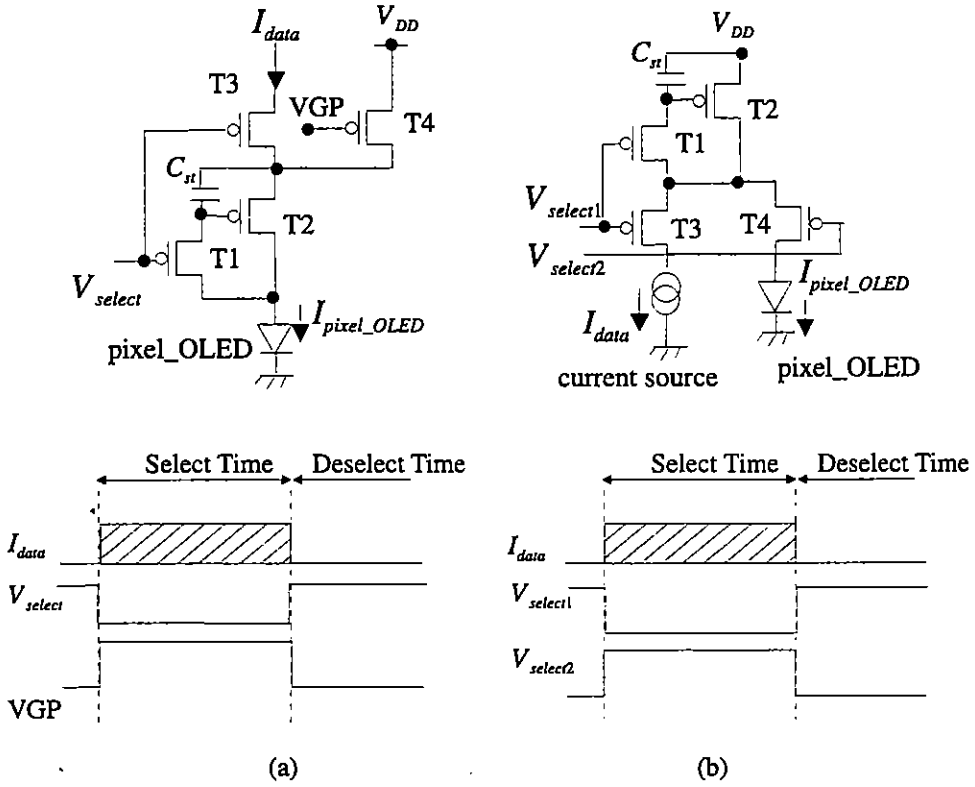

Figure 5.28 Two types of current-programming, current-driven pixel electrode circuits. The circuit in (a) was proposed by Dawson et al.[50] and the circuit in (b) by Ohta et al.[132]

These types of current-programmed OLED pixels may have charging time problems for data current at low gray scales in high-resolution display applications, although they can compensate for both the TFT's threshold voltage and field-effect mobility variations, and for the OLED threshold voltage shift. The data current must first charge up the parasitic capacitance formed between the data lines and cathode before the current is written onto a specific pixel within select time. Therefore, the actual charging process of each pixel cannot be completed within select time since the parasitic capacitance increases as the number of pixels increases.

To solve this charging time issue in current-driven AM driving methods, Sony Corporation[147] introduced a current-mirror type of pixel electrode circuit with two n-type (T3 and T4) and two p-type poly-Si TFTs (T1 and T2), as shown in Fig. 5.29(a). T3 and T4 are switching TFTs, and T1 and T2 form back-to-back transistors of the current mirror. During select time, the write (Write scan) and erase (Erase scan) scan lines are high, and the data current flows from V_{DD} through T1 and T3 to the I_{data} line. At the same time, I_{pixel_OLED} flows from V_{DD} through T2 to pixel_OLED, and the pixel_OLED emits light. By setting the channel width of T1 larger than that of T2, the data current is larger than the I_{pixel_OLED}, which makes the write operation fast enough even at a low gray scale. During deselect time, the write scan is low and

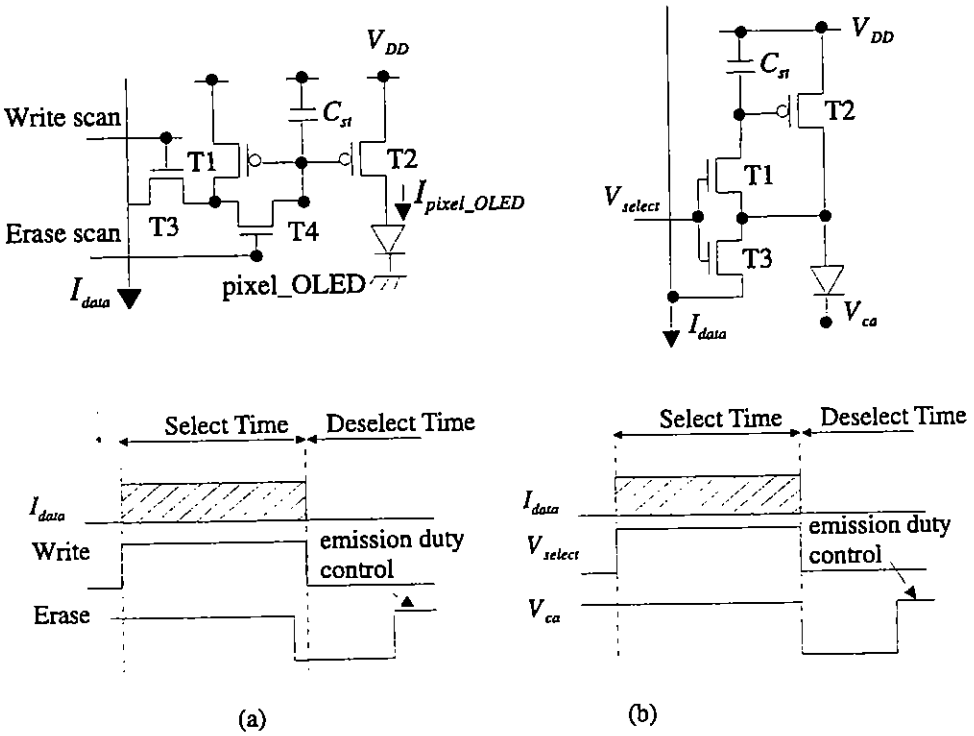

Figure 5.29 Two types of current-mirror, current-driven pixel electrode circuits for AMOLEDs, proposed by (a) Sasaoka et al.[147] and (b) Fish et al.[56]

T1 is off. The same amount of I_{pixel_OLED} continuously flows through the pixel_OLED; a continuous light-emission can be achieved because C_{st} determines the I_{pixel_OLED} level, and T2 operates in the saturation regime during deselect time. Sony introduced an erase scan line to obtain a secure write operation by turning T4 off slightly earlier than T3. The erase scan can also control the time-averaged pixel brightness and the pixel emission duty by turning T4 on during deselect time. The pixel emission duty control produces a high-quality, fast-moving image.

Philips Research Laboratories[56] also reported a modified current-mirror type of pixel electrode circuit with two n-type and one p-type poly-Si TFTs, as shown in Fig. 5.29(b). T1 and T3 are switching TFTs, and T2 is a driving TFT. During select time, V_{select} is high, T1 and T3 are on, and the data current flows from V_{DD} through T1 and T3 to the I_{data} line, thus charging C_{st} to a level corresponding to the data-current level. No current flows through pixel_OLED because V_{ca} is high during select time. Then, during deselect time, V_{select} is low, T1 and T3 are off, the same amount of current flows from V_{DD} through T2 to the pixel_OLED, and pixel_OLED emits light. The stored charge in the storage capacitor determines the current level, and T2 operates in the saturation regime during deselect time. Philips used a pulsed cathode voltage approach (V_{ca}) to operate the pixel electrode circuit at an efficient pixel_OLED operating point. This pulsed cathode voltage approach has other advantages, such

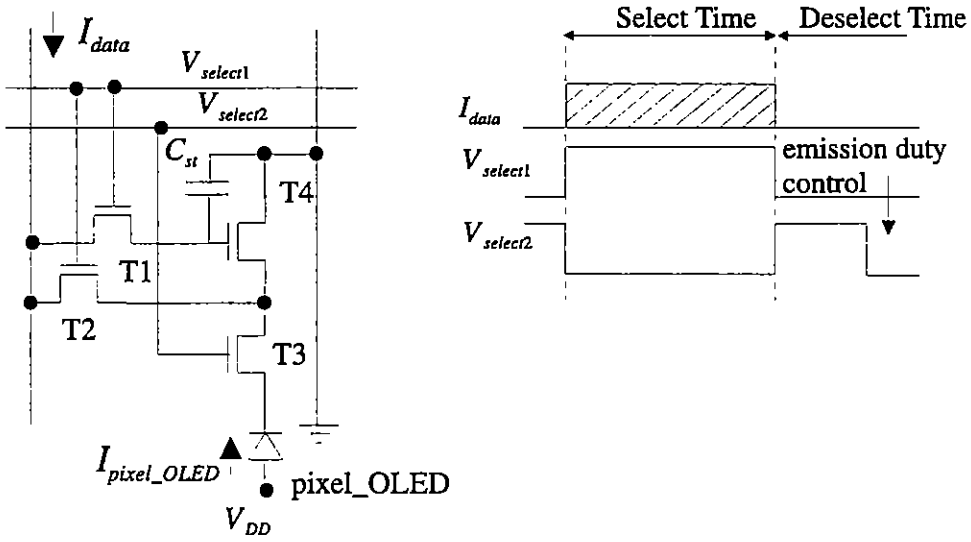

Figure 5.30 A current-sink, current-driven pixel electrode circuit proposed by Hong et al.[83]

as a higher programming current and an emission duty control for an improved motion image.

Kanicki's research group[83] also reported a current-sink pixel electrode circuit with four n-type poly-Si TFTs, as shown in Fig. 5.30. T1 and T2 are selecting TFTs, and T3 and T4 are switching and driving TFTs, respectively. The T1/T2 and T3 TFTs control the current flow path according to appropriate selecting voltage signals. During select time, T1and T2 are on and T4 is off, directing the data current flow from the data line to the source line (GND) through T2 and T3. After the storage capacitor is charged up during select time, the $V_{select1}$ and $V_{select2}$ signals change during frame time, turning T1 and T2 off and T4 on, respectively. Then the data current will flow from V_{DD} to ground through the OLED, T_3, and T_4. The $V_{select2}$ waveform can be appropriately selected for a higher programming current and an emission duty control, which produces a high-quality, fast-moving image. This pixel electrode circuit requires a top-anode pixel_OLED structure as shown in Fig. 5.31(b).

It is noted that all the above voltage-driven and current-driven pixel electrode circuits are based on poly-Si TFT technology. For large-area, low-cost, high-resolution displays, the poly-Si TFT AMOLED can be challenged by a low-cost a-Si:H TFT AMOLED based on the AM arrays developed for AMLCDs. One example of such a pixel electrode circuit is shown in Fig. 5.32. This a-Si:H TFT circuit was developed in Kanicki's research group.[85] The four-TFT pixel circuit can provide continuous current even after the pixel is deselected; and the TFT threshold voltage variations, which occur due to process variations and operational stress, are fully compensated in this circuit. The circuit has four external connections: V_{DD}, V_{select}, I_{data}, and ground (also the OLED cathode). As shown in the figure, TFT T5 and C_{diode} are used to schematically represent the OLED.

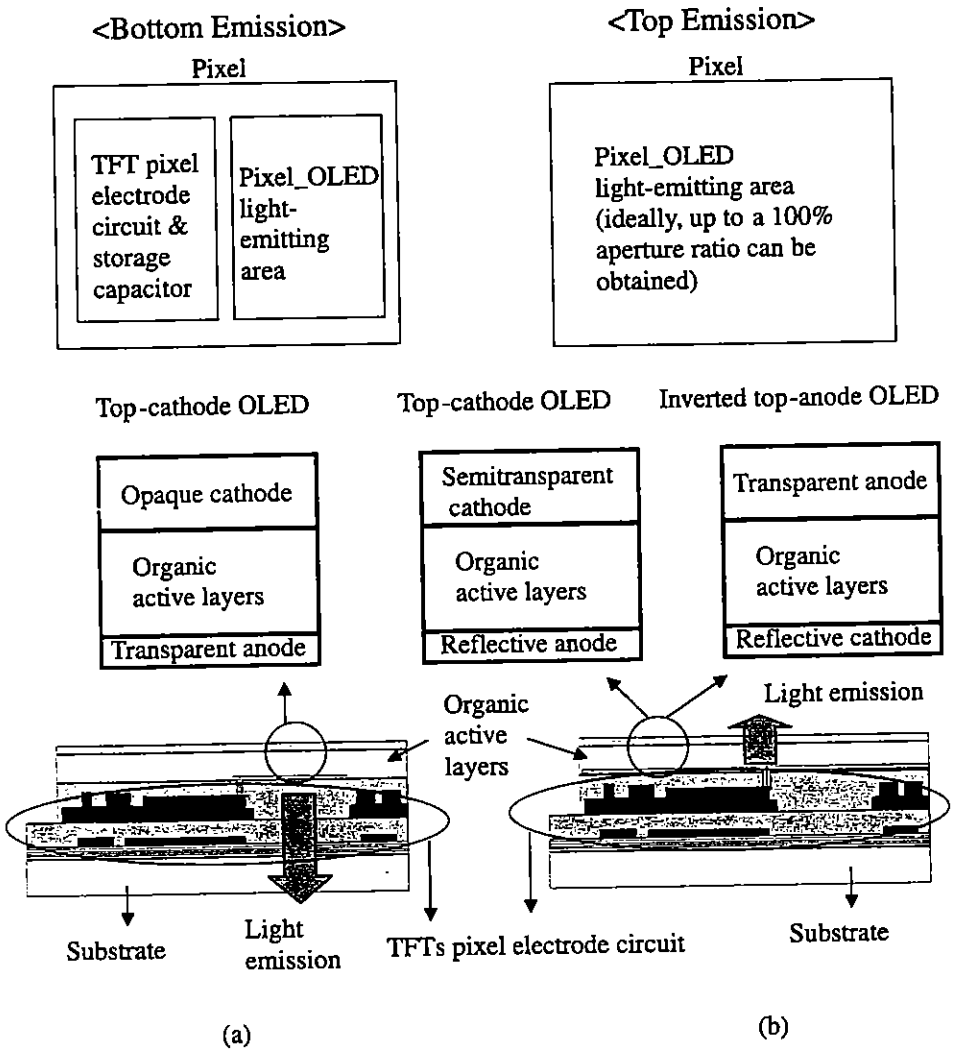

Figure 5.31 Bottom-emission and top-emission pixel electrode circuit configurations.

First we will describe the "on" (pixel selected) state. When the V_{select} signal is made high, the switching TFTs, T1 and T2, are turned on. The data signal current, from I_{data}, passes through T1 and T2, thereby storing charge on the storage capacitor and setting the drain and gate biases of the drive TFT (T3). This allows the data current to pass through T3. The value of V_{DD} has been chosen so that it is lower than the bias on the drain of T3, ensuring that no current can flow through TFT T4. This guarantees that all of the data current, I_{data}, which passes through T3, then goes through T5 (OLED) to ground. When the pixel is deselected (the "on" state), the select line bias is made low. This turns the switching TFTs, T1 and T2, off. The charge on the storage capacitor maintains the bias on the gate of T3. Therefore, current still flows through T3, causing the bias on the drain of T3 to

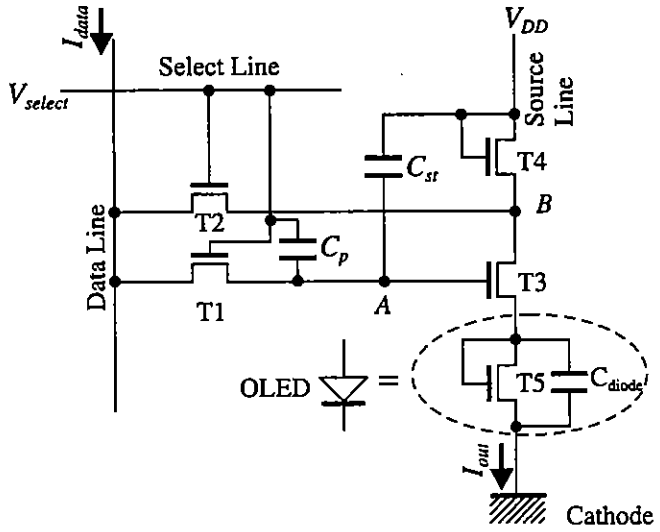

Figure 5.32 Equivalent pixel electrode circuit of a four a-Si:H TFT proposed by He et al.[75, 77] © J. Kanicki.

drop rapidly. When the bias on the drain of T3 drops below V_{DD}, T4 will turn on and maintain a constant current through T3. In this state, the current flows from V_{DD}, through T4 and T3, and then through T5 (OLED) to ground. Even in the "on" state, the required data current through the OLED is maintained. [76, 84]

It is possible, through process variations and operational device stress, that the threshold voltage of the drive transistor T3 can change. The four-TFT pixel circuit can compensate for such changes through the following mechanisms. Since T1, T2, and T4 are used as switches and are not used to control the output current, threshold voltage variations in these TFTs will not affect the output current.[77] However, if the threshold voltage of T3 changes, the gate bias must be changed in order to maintain the desired amount of output current. Since I_{data} is forced through T3, the gate voltage of T3 adjusts to maintain this amount of current, regardless of the value of the threshold voltage. Therefore, the threshold voltage variation of T3 will not affect the level of output current.[77, 78] This pixel electrode circuit with some modifications, as described in Ref. [78], was used to produce a-Si:H TFT current-driven AMOLEDs.[85, 86] This driving pixel electrode circuit showed the ability to provide a pixel electrode brightness in excess of 1000 cd/m^2 for a typical OLED with an external efficiency of 1%.

Although each pixel electrode circuit has its advantages and disadvantages, their operating principles can be categorized under two main types—voltage-driven and current-driven AMOLED driving schemes—as shown in Table 5.6. In both driving schemes, the driving TFT typically operates in the saturation regime to compensate for voltage variations. The voltage-driven pixel electrode circuits can be combined easily with a commercially available AMLCD data voltage driver. However, as previously noted, they are limited to fully compensating for TFT

Table 5.6 Comparison between voltage-driven and current-driven AMOLED driving schemes.

Property	Voltage-driven AMOLED	Current-driven AMOLED
Data signal	Voltage	Current
Data signal driver	Commercially available (AMLCD driver can be used)	Under development (standardization may be required)
Slow charging time an issue at low display brightness levels?	No	Yes (can be solved by current-mirror or current-sink type structure)
TFT threshold voltage compensation?	Yes (complicated threshold voltage memory steps are required during select time)	Yes
TFT field-effect mobility compensation?	No	Yes
OLED threshold voltage compensation?	Yes (by the driving TFT)	Yes (by both the driving TFT and direct current writing)

field-effect mobility variations. In addition, rather complicated control signals are required to write the TFT threshold voltage information onto each pixel. For the current-driven pixel electrode circuits, specific data current drivers are needed for each pixel electrode circuit configuration. The magnitude of data current depends upon the display format and pixel electrode circuit design. Therefore, standardizing data current drivers is required for the commercial applications of the current-driven pixel electrode circuits, which may be very challenging. The issue of a slow charge at a low display brightness in the current-driven pixel electrode circuit can be solved by introducing a current-mirror and/or a current-sink type of pixel electrode structure. However, the direct writing of data current onto each pixel is a big advantage of the current-driven pixel electrode circuits, which can fully compensate for not only TFT and OLED threshold voltage shifts, but also for TFT field-effect mobility variations.

The pixel configuration is determined by the OLED structure. A typical OLED structure consists of a transparent anode, active organic layers, and an opaque cathode, which is necessary due to the process compatibility of the organic layers and the low work function of the metal cathode. Therefore, most of the mentioned pixel electrode circuits are combined with the opaque top-cathode structure; thus, the light emission is observed through the bottom transparent anode, as shown in Fig. 5.31(a). The bottom-emission type of pixel configuration has a limited pixel aperture ratio, which is closely related to the display power consumption and stability. The aperture ratio is defined by the ratio of the light-emitting area to the total pixel area. To increase the aperture ratio, Sony Corporation[147] adopted a

top-emission type of pixel configuration by using an opaque bottom-anode and semitransparent top-cathode pixel structure, as shown in Fig. 5.31(b). Ideally, this approach can produce up to a 100% aperture ratio. Since the light emission in this approach is observed through the semitransparent cathode, a certain amount of light will be lost. Therefore, if an equivalent OLED performance is obtained for an inverted device structure (opaque cathode/active organic layers/transparent anode) in comparison with the conventional OLED structure, the top-emission pixel configuration with a transparent top-anode pixel_OLED structure could be very beneficial for future AMOLEDs. The current-sink type of pixel electrode circuit[83] can also be combined with this transparent top-anode structure, as shown in Fig. 5.31(b).

5.7 Methods to Improve AMOLED Contrast Ratio

The high reflectance of the OLED metal alloy cathode can lead to a low pixel contrast ratio (PCR) in high-ambient illuminance.[70] Here, we quantify the PCR by defining the discrimination ratio as the ratio of the brightness of an "on" pixel to that of an "off" pixel. The brightness of an "off" OLED is taken to be solely due to the reflection of the ambient illuminance, E_a, which is assumed to have a uniform angular distribution. Therefore, the "off" pixel brightness is $L_{off} = RE_a/2\pi$, where R is the reflectance of the pixel measured from the substrate side. The "on" pixel brightness is $L_{on} = L_d + L_{off}$. The discrimination ratio is, therefore, $D = 1 + (2\pi L_d/RE_a)$, which is plotted in Fig. 5.33 as a function of display reflectance R under E_a = 500 lux (ANSI standard) for different display brightnesses (L_d). For L_d = 100 cd/m^2 and R = 80%, D = 2.6. Discrimination ratios larger than 5 can only be achieved with a display brightness larger than 200 cd/m^2 for high-reflectance pixels under specific ambient lighting conditions. To increase D, the reflection of ambient light must be suppressed.

A circular polarizer (CP) can be placed in front of the display to achieve high discrimination ratios. Although the quarter-wave plate in the CP is wavelength dependent, the reflected ambient light can be sufficiently attenuated if the quarter-wave plate is centered near λ = 555 nm, where $V(\lambda)$ (the relative spectral luminous efficiency function for photopic vision) is maximum. This is due to the broad spectral width of the CP blocking band coupled with the eye's insensitivity to the wavelengths in the tails of $V(\lambda)$. A 0^{th}-order quarter-wave plate is desirable to obtain a broad blocking band for the CP.

To analyze the improvement in PCR associated with proposed schemes, it is assumed that the front surface of the display is AR coated, and thus the Fresnel reflections at this surface can be neglected. Here, the front of the display is the polarizer surface facing the viewer. Assuming a uniform spectral distribution for the ambient illuminance, a zeroth-order quarter-wave plate centered at λ =555 nm and a 100% efficiency for the CP, the luminance due to reflected ambient light is found to be attenuated by a factor of 71, while the emitted light is attenuated by

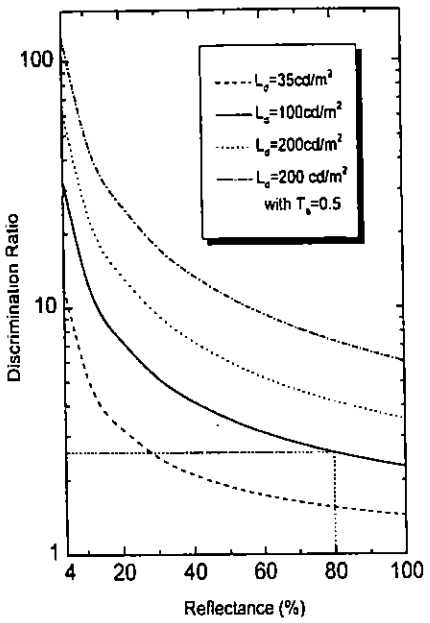

Figure 5.33 Discrimination ratio versus OLED reflectance curves under a 500-lux ambient illuminance. Reprinted from Ref. [70] with permission of the IEEE.

only a factor of 2. Hence, for a display with L_d = 200 cd/m^2 (corresponding to a 100 cd/m^2 perceived brightness) and 80% efficiency under a 500-lux ambient illuminance, D is increased to 113.

5.8 Current Market and Future Trends

According to one source,[40] FPDs are a potential $20 billion (U.S. currency) annual market, with about 50% in wireless applications. FPD applications include cell phones, personal digital assistants (PDAs), monitors, and televisions. Annual growth is projected to be 15 to 30% depending on the specific application. In five years, experts estimate that the market could reach $55 billion. According to a display market research firm, Stanford Resources, the worldwide OLED display market is forecasted to increase from several hundred thousand units valued at $3 million in 1999 to more than 100 million units valued at $714 million in 2005. Table 5.7 shows the current and future OLED markets by application.

5.8.1 Comparison between OLED and non-LED displays

The light output of an OLED display is Lambertian, which means the user can view the display from any angle (up to 160 deg) with the same perceived brightness. LCDs, however, are non-Lambertian displays whose image interference pat-

Table 5.7 Worldwide OLED market[a] by application.[b]

Application	2000	2001	2002	2003	2004	2005
Audio	1161	2712	4174	6078	8109	8822
Automobile displays	373	1587	3158	6028	10,035	12,868
Cell phones	60	277	1058	2387	3998	5678
Appliances	1037	2870	6909	13,484	20,656	26,091
Meters/multimeters	910	2005	3495	4776	5745	7220
ATM/cash registers	520	2102	4923	8401	11,474	15,958
Telephones	130	889	1630	2911	4251	6713
Test equipment	360	576	975	1477	2089	2428
VCR/cable boxes	229	1053	2257	3600	5298	7251

[a] Unit shipments given in thousands.

[b] Adapted from Ref. [119] with permission of iSuppli/Stanford Resources.

tern changes as the viewer's eye moves. The eye then perceives a different image, including a different color balance.

OLED displays are low-power displays that use thin organic films as the light emitters, thereby eliminating the need for power-hungry backlights and their environmentally unfriendly mercury content. In conventional LCDs, the backlights are on all the time at full power; but with OLEDs, the individual pixels are turned on and off as they are needed, thereby using only approximately half the power consumption of an LCD. In addition, LCDs are not photoactive. They act as light filters and require back lighting. Only 30 to 35% of the backlight passes through an LCD. As a result, LCDs consume a tremendous amount of power: up to 60% of the drain on a laptop battery is from the LCD.

Currently, efficiencies of the best doped-polymer and molecular OLEDs already exceed that of incandescent light bulbs. Efficiencies of 20 lm/W have been reported for yellow- and green-emitting polymer devices, and 40 lm/W has been attained for phosphorescent molecular OLEDs—compared to less than 20 lm/W for a typical incandescent light bulb. It is reasonable to predict that soon, efficiencies of 80 lm/W (a value comparable to that of fluorescent room lighting) will be achieved using phosphorescent OLEDs.

Not only does the lack of a backlight in OLEDs lengthen the battery life and minimize heat and electric interference, but it also reduces the overall size and weight of the end product. As glass-based displays, LCDs are prone to breakage and can be heavy for small portable applications. A complete poly-OLED display is less than 2 mm thick, weighs approximately 0.1 ounces, and requires a low operating voltage of only 2 to 6 V.

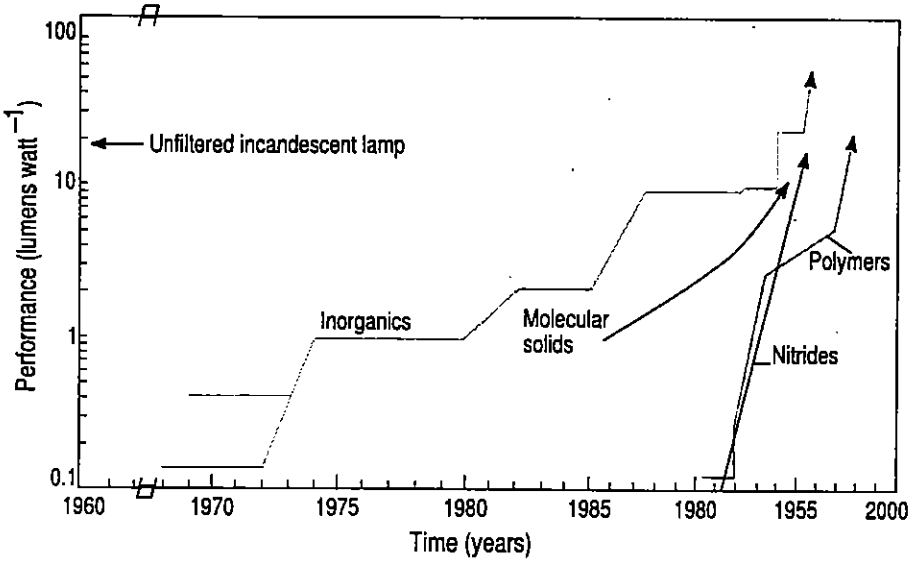

Figure 5.34 Comparison between OLEDs and inorganic LEDs. Reprinted from Ref. [171] with permission of Nature/Macmillan.

5.8.2 Comparison between OLEDs and inorganic LEDs

LEDs based on crystalline inorganic semiconductors have a long history, and their performance has improved steadily since their invention. It is when viewed in this context that the recent progress made with semiconducting organic materials seems so remarkable.

Figure 5.34 shows the evolution of organic and inorganic LEDs with performance given in lumens per watt (a typical value for an unfiltered incandescent lamp is shown for comparison). Inorganic LEDs based on III-V semiconductors such as gallium arsenide arrived on the scene in the early 1960s, and their performance has shown steady but significant progress since that time. Organic LEDs appeared much more recently, yet are already approaching the best performance levels of their inorganic counterparts. The nitride-based semiconductors are another success story and have extended applications of inorganic LEDs into the blue-violet region of the spectrum.

5.8.3 Current and future challenges

Even though OLED display technology enjoys tremendous advantages over traditional inorganic LED and other display technologies such as LCDs, it is not yet ready for batch fabrication and a competitive display market. Several challenges must be overcome.

First, manufacturing difficulties must be reduced.[64] Researchers have encountered many difficulties in manufacturing devices with the thin layers needed to achieve operating voltages between 5 and 10 V. OLEDs are vulnerable to electrical shorts caused by pinhole defects in the film or contamination of the substrate surface by dust particles. Furthermore, the materials tend to be mechanically fragile and are easily attacked by the chemicals used in photolithographic patterning. Therefore, patterning often requires low-resolution methods such as defining the device contact by metal deposition through a shadow mask, often in combination with costly dry-processing techniques. In the future, however, many new lithographic patterning techniques could appear, and even techniques borrowed from other industries such as injection molding, direct imprinting using stamping, and ink-jet printing.

Second, researchers are racing to find ways to effectively combine OLEDs that emit at different color bands into a single full-color display. This is a formidable task. The materials are generally better suited for the deposition of large-area, uniform layers rather than intricately patterned arrays of differently colored pixels; and the emission colors (and efficiencies) of the individual pixels need to be carefully balanced to match the spectral response of the eye. For the molecular systems, vacuum deposition through a patterned "mask" provides a promising route for achieving the necessary control. Prototype 5- to 20-in. displays based on this approach were exhibited by many different companies. Solution-based polymers are not amenable to vapor-phase deposition, so alternative strategies must be explored. The ink-jet technique (as used in color printers) is one possible avenue for producing the necessary pixel arrays, although the initial results suggest that further optimization of this process is needed.

Third, the display market is already well served by several more established technologies, so competition will be stiff. For the cruder monochrome applications, the combination of low power consumption, simplicity of fabrication, and the "gimmick" factor of having an unusually colored display could well be sufficient to give organic LEDs a competitive edge. The situation with full-color displays is harder to predict and, in the short term, they will need to demonstrate a cost advantage if they are to succeed. But in the long term, properties unique to the organic systems (as discussed in previous sections) may come to the fore, and as mentioned above, it is conceivable that within five years, we will have flexible color displays that can be rolled up and put in our pockets.

Finally, although current efforts for commercialization of OLED technology are focused on flat-panel displays, other applications are being investigated. The OLED technology could be used for outdoor and emergency lighting conditions and should be capable of running on full speed at very low temperatures (–40°C or less). This display technology could also be used for cell phones, digital still cameras, camcorders, personal digital assistants, head-wearable displays, and car navigation systems. Also, today flexible OLEDs are being heavily investigated so that one day e-books based on AMOLED technology can substitute for the paper-version books that have been used for thousands of years.

References

[1] J. W. Allen, "Organic electroluminescence and competing technologies," *Journal of Luminescence* **60-61**, pp. 906–911 (1994).

[2] American College of Radiology/National Electrical Manufacturers Assoc. (ACR/NEMA) technical report, *Digital Imaging and Communications in Medicine (DICOM), Part 3.14, Grayscale Standard Display Function* (January 1998).

[3] V. I. Arkhipov, E. V. Emelianova, Y. H. Tak, and H. Bässler, "Charge injection into light-emitting diodes: theory and experiment," *Journal of Applied Physics* **84**, pp. 848–856 (1998).

[4] A. Badano, "Image Quality Degradation by Light Scattering Processes in High Performance Display Devices for Medical Imaging," Ph.D. thesis, University of Michigan (1999).

[5] A. Badano, "Modeling the bidirectional reflectance of emissive displays," *Applied Optics* **42(19)**, pp. 3847–3852 (2002).

[6] A. Badano, "Principles of cathode ray tube and liquid crystal display devices," *Advances in Digital Radiography: RSNA Categorical Course in Diagnostic Radiology Physics*, pp. 91–102, Radiological Society of North America, Oak Brook, IL (2003).

[7] A. Badano, S. Drilling, B. Imhoff, R. J. Jennings, R. M. Gagne, and E. Muka, "Noise in flat-panel displays with sub-pixel structure," *Medical Physics*, in press.

[8] A. Badano and M. J. Flynn, "A method for measuring veiling glare in high performance display devices," *Applied Optics* **39(13)**, pp. 2059–2066 (2000).

[9] A. Badano and M. J. Flynn, "Monte Carlo modeling of the luminance spread function in flat panel displays," *International Display Research Conference* **17**, pp. 382–385, Society for Information Display, San Jose, CA (1997).

[10] A. Badano, M. J. Flynn, and J. Kanicki, "Accurate small-spot luminance measurements," *Displays* **23**, pp. 177–182 (2002).

[11] A. Badano, M. J. Flynn, and J. Kanicki, "Small spot contrast measurements in high-performance displays," *Proc. of the 1999 SID International Symposium*, pp. 516–519 (1999).

[12] A. Badano, M. J. Flynn, S. Martin, and J. Kanicki, "Angular dependence of the luminance and contrast in medical imaging monochrome active-matrix liquid crystal displays," *Medical Physics* **30(10)**, pp. 2602–2613 (2003).

[13] A. Badano, M. J. Flynn, E. Muka, K. Compton, and T. Monsees, "Veiling glare point-spread function of medical imaging monitors," *SPIE Proc.* **3658**, pp. 458–467 (1999).

[14] A. Badano, S. J. Hipper, and R. J. Jennings, "Luminance effects on display resolution and noise," *SPIE Proc.* **4681**, pp. 305–313 (2002).

[15] A. Badano and J. Kanicki, "Characterization of crosstalk in high-resolution active-matrix liquid crystal displays for medical imaging," *SPIE Proc.* **4295**, pp. 248–253 (2001).

[16] A. Badano, S.-J. Lee, J. Kanicki, E.F. Kelley, and R.J. Jennings, "Bidirectional reflectance of organic light-emitting displays," *International Display Research Conference* **21**, pp. 21–24 (2001).

[17] M. A. Baldo, M. E. Thompson, and S. R. Forrest, "High-efficiency fluorescent organic light-emitting devices using a phosphorescent sensitizer," *Nature* **403**, pp. 750–753 (2000).

[18] P. G. J. Barten, *Contrast Sensitivity of the Human Eye and its Effect on Image Quality*, **PM 72**, SPIE Press, Bellingham, WA (1999).

[19] P. G. J. Barten, "Effects of quantization and pixel structure on the image quality of color matrix displays," *Journal of the SID* **1(2)**, pp. 147–153 (1993).

[20] P. G. J. Barten, "Physical model for the contrast sensitivity of the human eye," *SPIE Proc.* **1666**, pp. 57–72 (1992).

[21] P. G. J. Barten, "Subjective image quality of HDTV pictures," *International Display Research Conference* **19**, p. 598 (1989).

[22] B. Baxter, H. Ravindra, and R. A. Normann, "Changes in lesion detectability caused by light adaptation in retinal photoreceptors," *Investigative Radiology* **17**, pp. 394–401 (1982).

[23] D. A. Baylor and M. G. F. Fuortes, "Electrical responses of single cones in the retina of the turtle," *Journal of Physiology* **207**, pp. 77–92 (1970).

[24] M. E. Becker, "Evaluation and characterization of display reflectance," *Displays* **19**, pp. 35–54 (1998).

[25] C. Beckman, O. Nilsson, and L.-E. Paulsson, "Intraocular light scattering in vision, artistic painting, and photography," *Applied Optics* **33(21)**, pp. 4749–4753 (July 1994).

[26] M. Berggren, A. Dodabalapur, R. E. Slusher, and Z. Bao, "Light amplification in organic thin films using cascade energy transfer," *Nature* **389**, pp. 466–469 (1997).

[27] M. T. Bernius, M. Inbasekaran, J. O'Brien, and W. Wu, "Progress with light-emitting polymers," *Advanced Materials* **12(23)**, pp.1737–1750 (2000).

[28] A. Bernsten, Y. Croonen, C. Liedenbaum, H. Schoo, R. J. Visser, J. Vleggaar, et al., "Stability of polymer LEDs," *Optical Materials* **9**, pp. 125–133 (1998).

[29] A. Bernsten, P. van de Weijer, Y. Croonen, C. Liedenbaum, and J. Vleggaar, "Stability of polymer light-emitting diodes," *Philips Journal of Research* **51**, pp. 511–525 (1998).

[30] H. Blume and B. M. Hemminger, "Image presentation in digital radiology: perspectives on the emerging DICOM display function standard and its application," *Radiographics* **17**, pp. 769–777 (1997).

[31] M. Born and E. Wolf, *Principles of Optics, Third Edition*, Pergamon Press, London (1965).

[32] R. W. Boyd, *Radiometry and the Detection of Optical Radiation*, John Wiley & Sons, New York (1983).

[33] D. Braun, "Crosstalk in passive matrix polymer LED displays," *Synthetic Metals* **92**, pp. 107–113 (1998).

[34] R. Brinkley, G. Xu, A. Abileah, R. Brinkley, G. Xu, A. Abileah, et al., "Wide-viewing-angle AMLCD optimized for gray-scale operation," *Proc. of the Society for Information Display* **29**, pp. 471–474 (1998).

[35] P. L. Burn, A. B. Holmes, and A. Kraft, "Chemical tuning of electroluminescent copolymers to improve emission efficiencies and allow patterning," *Nature* **356**, pp. 47–49 (1992).

[36] J. H. Burroughes, D. D. C. Bradley, A. R. Brown, R. N. Marks, K. Mackay, R. H. Friend, et al., "Light-emitting diodes based on conjugated polymers," *Nature* **347**, pp. 539–541 (1990).

[37] P. E. Burrows, V. Bulovic, S. R. Forrest, L. S. Sapochak, D. M. McCarty, and M. E. Thompson, "Reliability and degradation of organic light emitting devices," *Applied Physics Letters* **65(23)**, pp. 2922–2924 (1994).

[38] P. E. Burrows, G. Gu, V. Bulovic, Z. Shen, S. R. Forrest, and M. E. Thompson, "Achieving full-color organic light-emitting devices for lightweight, flat-panel displays," *IEEE Transactions on Electron Devices* **44(8)**, pp. 1188–1203 (1997).

[39] P. E. Burrows, Z. Shen, and S. R. Forrest, "Saturated full color stacked organic light emitting devices," *International Display Research Conference* **17**, pp. 318–321 (1997).

[40] C. Challener, "Fast-growing polymer-OLED market is pursued by major chemical players," *Chemical Market Reporter* **258**, pp. 22–23 (2000).

[41] C.-Y. Chen and J. Kanicki, "High field-effect mobility a-Si:H TFT based on high deposition-rate PECVD materials," *IEEE Transactions on Electron Devices* **17**, pp. 437–439 (1996).

[42] J. Chen, P. J. Bos, D. R. Bryant, D. L. Johnson, S. H. Jamal, and J. R. Kelly, "Four-domain TN-LCD fabricated by reverse rubbing or double evaporation," *Proc. of the Society for Information Display* **26**, pp. 865–868 (1995).

[43] J. Chen, K.-H. Kim, J.-J. Jyu, J. H. Souk, J. R. Kelly, and P. J. Bos, "Optimum film compensation modes for TN and VA LCDs, *Proc. of the Society for Information Design 1998*, pp. 315–318 (1998).

[44] X. Cheng, Y. Hong, J. Kanicki, and L. J. Guo, "High-resolution organic polymer light-emitting pixels fabricated by imprinting technique," *J. Vac. Sci. Technol. B* **20(6)**, pp. 2877–2880 (2002).

[45] P. J. Collings, *Liquid Crystals, Nature's Delicate Phase of Matter*, A. Hilger, Bristol, England (1990).

[46] K. Compton, *Image Performance in CRT Displays,* SPIE Press, Vol. TT54, Bellingham, WA (2003).

[47] B. K. Crone, P. S. Davids, I. H. Campbell, and D. L. Smith, "Device model investigation of single layer organic light emitting diodes," *Journal of Applied Physics* **84**, pp. 833–842 (1998).

[48] S. Daly, "The visible differences predictor: an algorithm for the assessment of image fidelity," in *Digital Images and Human Vision*, Andrew B. Watson, Editor, pp. 179–206, MIT Press, Cambridge, MA (1993).

[49] R. M. A. Dawson, Z. Shen, D. A. Furst, S. Connor, J. Hsu, M. G. Kane, et al., "Design of an improved pixel for polysilicon active matrix organic LED display," *SID Tech. Dig.* **29**, pp. 11–14 (1998).

[50] R. M. A. Dawson, Z. Shen, D.A. Furst, S. Connor, J. Hsu, M.G. Kane, et al., "The impact of the transient response of organic light emitting diodes on the design of active matrix OLED displays," in *IEDM Tech. Dig.*, pp. 875–878 (1998).

[51] S. W. Depp and W. E. Howard, "Flat-panel displays," *Scientific American* **3(40)**, pp. 90–97 (March 1993).

[52] G. C. de Vries, "Contrast-enhancement under low ambient illumination," *Proc. of the Society for Information Display* **26**, pp. 32–35 (1995).

[53] P. Dyreklev, M. Berggren, O. Inganäs, M. R. Andersson, O. Wennerström, and T. Hjertberg, "Polarised electroluminescence from an oriented substituted polythiophene in a light emitting diode," *Advanced Materials* **7**, pp. 43–45 (1995).

[54] G. M. Ehemann, R. LaPeruta, and E. R. Garrity, "Method of Determining the Quality of an Aluminized, Luminescent Screen for a CRT," U.S. Patent No. 5,640,019 (1997).

[55] M. Elias, L. Simonot, and M. Menu, "Bidirectional reflectance of a diffuse background covered by a partly absorbing layer," *Optics Communications* **191**, pp. 1–7 (2001).

[56] D. Fish, N. Young, M. Childs, W. Steer, D. George, D. McCullock, et al., "A comparison of pixel circuits for active matrix polymer/organic LED displays," *SID Tech. Dig.* **33**, pp. 968–971 (2002).

[57] A. E. Flanders, R. H. Wiggins III, and M. E. Gozum, "Handheld computers in radiology," *Radiographics* **23**, pp. 1035–1047 (2003).

[58] Flat Panel Display Measurements Standard Working Group, Video Electronics Standards Association (VESA), *Flat Panel Display Measurements Standard, Version 2.0* (May 2003).

[59] M. J. Flynn, DisplayTool software, available upon request to mikef@rad.hfh.edu.

[60] M. J. Flynn and A. Badano, "Image quality degradation by light scattering in display devices," *Journal of Digital Imaging* **12(2)**, pp. 50–59 (May 1999).

[61] M. J. Flynn, Jerzy Kanicki, Aldo Badano, and William R. Eyler, "High-fidelity electronic display of digital radiographs," *Radiographics* **19(6)**, pp. 1653–1669 (1999).

[62] M. J. Flynn, T. McDonald, E. G. DiBello, J. L. Jorgensen, and W. Worobey, "Flat panel display technology for high performance radiographic imaging," *SPIE Proc.* **2431**, pp. 360–371 (1995).

[63] S. R. Forrest, P. E. Burrows, Z. Shen, G. Gu, V. Bulovic, and M. E. Thompson, "The stacked OLED (SOLED): a new type of organic device for achieving high-resolution full-color displays," *Synthetic Metals* **91**, pp. 9–13 (1997).

[64] S. R. Forrest, P. E. Burrows, and M. E. Thompson, "The dawn of organic electronics," *IEEE Spectrum* **37(8)**, pp. 29–34 (2000).

[65] R. H. Fowler and L. Nordheim, "Electron emission in intense electric fields," *Proc. Roy. Soc. London* **119A**, pp. 173–181 (1928).

[66] M. Fujihira, L. M. Do, A. Koike, and E. M. Han, "Growth of dark spots by interdiffusion across organic layers in organic electroluminescent devices," *Applied Physics Letters* **68(13)**, pp. 1787–1789 (1996).

[67] Y. Fukuda, T. Watanabe, T. Wakimoto, S. Miyaguchi, and M. Tsuchida, "An organic LED display exhibiting pure RGB colors," *Synthetic Metals* **111-112**, pp. 1–6 (2000).

[68] R. E. Gill, P. van de Weijer, C. T. H. Liedenbaum, H. F. M. Schoo, A. Berntsen, J. J. M. Vleggaar, et al., "Stability and characterization of large area polymer light-emitting diodes over extended periods," *Optical Materials* **12(2-3)**, pp. 183–187 (1999).

[69] N. C. Greenham, S. C. Moratti, D. D. C. Bradley, R. H. Friend, and A. B. Holmes, "Efficient light-emitting diodes based on polymers with high electron affinities," *Nature* **365**, pp. 628–630 (1993).

[70] G. Gu and S. R. Forrest, "Design of flat-panel displays based on organic light-emitting devices," *IEEE Journal on Selected Topics in Quantum Electronics* **4(1)**, pp. 83–99 (1998).

[71] R. W. Gymer, "Organic electroluminescent displays," *Endeavour* **20**, pp. 115–120 (1996).

[72] M. Hack, R. Kwong, M. S. Weaver, M. Lu, and J. J. Brown, "Active-matrix technology for high efficiency OLED displays," in *Proc. of IDMC '02*, pp. 57–60 (2002).

[73] T. B. Harvey III, Q. Shi, and F. So, "Passivated Organic Device having Alternating Layers of Polymer and Dielectric," U.S. Patent No. 5,757,126 (May 1998).

[74] F. Hasselbach and H.-R. Krauss, "Backscattered electrons and their influence on contrast in the scanning electron microscope," *Scanning Microscopy* **2(2)**, pp. 1947–1956 (1988).

[75] Y. He, "Polyfluorene Light-Emitting Devices and a-Si:H TFT Pixel Circuits for Active-Matrix Organic Light Emitting Displays," Ph.D. thesis, University of Michigan (2000).

[76] Y. He, S. Gong, R. Hattori, and J. Kanicki, "High performance organic polymer light-emitting heterostructure devices," *Applied Physics Letters* **74**, pp. 2265–2267 (1999).

[77] Y. He, R. Hattori, and J. Kanicki, "Current-source a-Si:H thin-film transistor circuit for active-matrix organic light-emitting displays," *IEEE Electron Device Letters* **21(12)**, pp. 590–592 (2000).

[78] Y. He, R. Hattori, and J. Kanicki, "Improved a-Si:H TFT pixel electrode circuits for active-matrix organic light emitting displays," *IEEE Transactions on Electron Devices* **48(7)**, pp. 1322–1325 (2001).

[79] S. Hecht and Y. Hsia, "Dark adaptation following light adaptation to red and white lights," *Journal of the Optical Society of America* **35(4)**, pp. 261–267 (April 1945).

[80] S. Hecht and Y. Hsia, "Relation between visual acuity and illumination," *Journal of General Physiology* **11**, pp. 255–281 (1928).

[81] P. K. H. Ho, J.-S. Kim, J. H. Burroughes, H. Becker, S. F. Y. Li, T. M. Brown, et al., "Molecular-scale interface engineering for polymer light-emitting diodes," *Nature* **404**, pp. 481–484 (2000).

[82] C. D. Hoke, H. Mori, and P. J. Bos, "An ultra-wide-viewing angle STNLCD with a negative-birefringence compensation film," *International Display Research Conference* **17**, pp. 21–24 (1997).

[83] Y. Hong, J. Kanicki, and R. Hattori, "Novel poly-Si TFT pixel electrode circuits and current programmed active-matrix driving methods for AM-OLED," *SID Tech. Dig.* **33**, pp. 618–621 (2002).

[84] Y. Hong, J.-Y. Nahm, and J. Kanicki, "100 dpi 4-a-Si:H TFTs active-matrix organic polymer light-emitting display," *IEEE Journal of Selected Topics in Quantum Electronics* **10**, pp. 16–25 (2004).

[85] Y. Hong, J.-Y. Nahm, and J. Kanicki, "Optoelectrical properties of four amorphous silicon thin-film transistors 200 dpi active-matrix organic polymer light-emitting display," *Applied Physics Letters* **83(16)**, pp. 3233–3235 (2003).

[86] Y. Hong, J.-Y. Nahm, and J. Kanicki, "200 dpi 4-a-Si:H TFTs current-driven AM-PLEDs," *SID '03 Digest*, pp. 22–25 (2003).

[87] ISO Technical Report 9241-7, *Ergonomic Requirements for Office Work with Visual Display Terminals* (1997).

[88] G. E. Jabbour, S. E. Shaheen, M. M. Morrell, B. Kippelen, N. R. Armstrong, and N. Peyghambarian, "Aluminum composite cathodes: a new method for the fabrication of efficient and bright organic light-emitting devices," *Optics and Photonics News* **10(4)**, p. 24 (1999).

[89] Y.-C. Jeong, C.-C. Park, and L.-S. Kim, "A new crosstalk compensation method in line inversion TFT-LCDs," *IEEE Transactions on Systems and Circuits*, **44(6)**, pp. 552–555 (1997).

[90] G. R. Jones, E. F. Kelley, and T. A. Germer, "Specular and diffuse reflection measurements of electronic displays," *Proc. of the Society for Information Display* **27**, pp. 203–206 (1996).

[91] G. W. Jones, W. E. Howard, and S. M. Zimmerman, "Sealing structure for organic light emitting devices," U.S. Patent No. 6,198,220 B1 (2001).

[92] E. Kaneko, *Liquid Crystal TV Display: Principles and Applications of Liquid Crystal Displays*, KTK Scientific Publishers, Tokyo (1987).

[93] J. Kanicki, Y. He, and R. Hattori, "a-Si:H pixel electrode circuits for AM-OLEDs," *SPIE Proc.* 4295, pp. 147–158 (2001).

[94] J. Kanicki, J. Lan, A. Catalano, J. Keane, W. Den Boer, and T. Gu, "Patterning of transparent conductive oxide thin films by wet etching for a-Si:H TFT-LCDs," *Journal of Electronic Materials* **25**, pp. 1806–1817 (1996).

[95] M. Kawasaki, N. Tani, and R. Onishi, "Improvement of contrast and brightness by using crystal pigment phosphor screens," *Proc. of the Society for Information Display* **29**, pp. 266–269 (1998).

[96] P. A. Keller, *The Cathode-Ray Tube: Technology, History and Applications*, Palisades Press, New York (1992).

[97] E. F. Kelley, "Display reflectance model based on BRDF," *Displays* **19**, pp. 27–34 (1998).

[98] J. Kido, K. Masato, and N. Katsutoshi, "Multilayer white light-emitting organic electroluminescent device," *Science* **267**, pp. 1132–1334 (March 1995).

[99] J. H. Kim, Y. Hong, and J. Kanicki, "Amorphous silicon thin-film transistors-based organic polymer light-emitting displays," *IEEE Electron Device Letters* **24(7)**, pp. 451–453 (2003).

[100] M. Kimura, I. Yudasaka, S. Kanbe, H. Kobayashi, H. Kiguchi, S. Seki, et al., "Low-temperature polysilicon thin-film transistor driving with integrated driver for high-resoluition light emitting polymer display," *IEEE Trans. Electron Devices* **46(12)**, pp. 2282–2288 (1999).

[101] Kodak, "Kodak, Sanyo unveil 15-inch flat-panel display," http://wwwnl.kodak.com/US/en/corp/display/sanyoFlat.jhtml, Chiba, Japan, posted October 2, 2002.

[102] K. Kohm, "Visual CRT sharpness estimation using a fiducial marker set," *SPIE Proc.* **4319**, pp. 286–297 (2001).

[103] H. Kubota, S. Miyaguchi, S. Ishizuka, T. Wakimoto, J. Funaki, Y. Fukuda, et al., "Organic LED full color passive-matrix display," *Journal of Luminescence* **87-89**, pp. 56–60 (2000).

[104] J.-H. Lan and J. Kanicki, "Planarized copper-gate hydrogenated amorphous silicon thin-film transistors for active-matrix liquid crystal displays," *IEEE Transactions on Electron Devices* **20(3)**, p. 129 (1999).

[105] S. Lee, A. Badano, and J. Kanicki, "Monte Carlo modeling of organic polymer light-emitting devices on flexible plastic substrates," *SPIE Proc.* **4800**, pp. 156–163 (2002).

[106] G. Leising, S. Tasch, F. Meghdadi, L. Athouel, G. Froyer, and U. Scherf, "Blue electroluminescence with ladder-type poly(para-phenylene) and parahexaphenyl," *Synthetic Metals* **81**, pp. 185–189 (1996).

[107] X. C. Li, F. Cacialli, M. Giles, J. Gruner, R. H. Friend, A. B. Holmes, et al., "Light-emitting-diodes based on Poly(Methacrylate)s with distyrylbenzene and oxadiazole side-chains," *Advanced Materials* **7**, pp. 898–900 (1995).

[108] F. R. Libsch and A. Lien, "A compensation driving method for reducing crosstalk in XGA and higher-resolution TFT-LCDs," *Proc. of the Society for Information Display* **26**, pp. 253–256 (1995).

[109] F. R. Libsch and A. Lien, "Understanding crosstalk in high-resolution color thin-film-transistor liquid crystal displays," *IBM Journal of Research and Development* **42(3/4)**, pp. 467–479 (May 1998).

[110] J.-J. Lih, C-F Sung, M. S. Weaver, M. Hack, and J. J. Brown, "A phosphorescent active-matrix OLED display driven by amorphous silicon backplane," *SID Tech. Dig.* **34**, pp. 14–17 (2003).

[111] S. F. Lim, K. Ke, W. Wang, and S. J. Chua, "Correlation between dark spot growth and pinhole size in organic light-emitting diodes," *Applied Physics Letters* **78**, pp. 2116–2118 (2001).

[112] M. Lindfors, "Accuracy and repeatability of the ISO 9241-7 test method," *Displays* **19**, pp. 3–16 (1998).

[113] C. J. Lloyd, M. Mizukami, and P. R. Boyce, "A preliminary model of lightning display interaction," *Journal of the Illuminating Engineering Society* **25(2)**, pp. 59–69 (1996).

[114] J. R. Mansell and A. W. Woodhead, "Contrast loss in image devices due to electrons back-scattered from the fluorescent screen," *Journal of Physics D: Applied Physics* **16**, pp. 2269–2278 (1983).

[115] S. Martin, A. Badano, and J. Kanicki, "Characterization of a high quality monochrome AM-LCD monitor for digital radiology," *SPIE Proc.* **4681**, pp. 293–304 (2002).

[116] Y. Masutani, S. Tahata, M. Hayashi, T. Onawa, K. Kobayashi, K. Nagata, et al., "Novel TFT-array structure for LCD monitors with in-plane switching mode," *Proc. of the Society for Information Display* **28**, pp. 15–18 (1997).

[117] J. McElvain, H. Antoniadis, M. R. Hueschen, J. N. Miller, D. M. Roitman, J. R. Sheats, et al., "Formation and growth of black spots in organic light-emitting diodes," *Journal of Applied Physics* **80**, pp. 6002–6007 (1996).

[118] Z. Meng and M. Wong, "Active-matrix organic light-emitting diode displays realized using metal-induced unilaterally crystallized polycrystalline silicon thin-film transistors," *IEEE Trans. Electron Devices* **49(6)**, pp. 991–996 (2002).

[119] D. Mentley, *Flat Panel Display Market Overview*, iSuppli/Stanford Resources (2002).

[120] D. E. Mentley, "State of flat-panel display technology and future trends," *Proc. of the IEEE* **90(4)**, pp. 453–459 (2002).

[121] A. A. Michelson, *Studies in Optics*, The University of Chicago Press, Chicago (1962).

[122] I. S. Millard, "High-efficiency polyfluorene polymers suitable for RGB applications," *Synthetic Metals* **111-112**, pp. 119–123 (2000).

[123] H. Mori and P. J. Bos, "Application of a negative birefringence film to various LCD modes," *International Display Research Conference* **17**, pp. M88–M97 (1997).

[124] E. Muka, T. Mertelmeier, and R. M. Slone, "Impact of phosphor luminance noise on the specification of high-resolution CRT displays for medical imaging," *SPIE Proc.* **3031**, pp. 210–221 (1997).

[125] S. Musa, "Active-matrix liquid-crystal displays," *Scientific American* **277**, pp. 87–92 (1997).

[126] M. S. Nam, J. W. Wu, Y. J. Choi, K. H. Yoon, J. H. Jung, J. Y. Kim, et al., "Wide-viewing-angle TFT-LCD with photoaligned four-domain TN mode," *Proc. of the Society for Information Display* **28**, pp. 933–936 (1997).

[127] J. A. Nichols, T. N. Jackson, M. H. Lu, and M. Hack, "a-Si:H TFT active-matrix phosphorescent OLED pixel," *SID Tech. Dig.* **33**, pp. 1368–1371 (2002).

[128] R. A. Norman, B. S. Baxter, and H. Ravindra, "Photoreceptor contributions to contrast sensitivity: Applications in radiological diagnosis," *IEEE Transactions on Systems, Man, and Cybernetics* **SMC-13(5)**, pp. 944–953 (1983).

[129] R. A. Norman and I. Perlman, "The effects of background illumination on the photoresponses of red and green cones," *Journal of General Physiology* **286**, pp. 491–507 (1979).

[130] R. A. Norman and F. S. Werblin, "Control of retinal sensitivity: light and dark adaptation of vertebrate rods and cones," *Journal of General Physiology* **63**, pp. 37–61 (1974).

[131] K. Ohmuro, S. Kataoka, T. Sasaki, and Y. Koike, "Development of super-high-image-quality vertical-alignment-mode LCD," *Proc. of the Society for Information Display* **28**, pp. 845–848 (1997).

[132] M. Ohta, H. Tsutsu, H. Takahara, I. Kobayashi, T. Uemura, and Y. Takubo, "A novel current programmed pixel for active matrix OLED displays," *SID Tech. Dig.* **34**, pp. 108–111 (2003).

[133] Y. Ono, Y. Ohtani, K. Hiratsuka, and T. Morimoto, "A new antireflective and antistatic double-layered coating for CRTs," *Proc. of the Society for Information Display* **23**, pp. 511–514 (1992).

[134] L. Ozawa, *Cathodoluminescence: Theory and Applications*, Kodansha, Tokyo (1990).

[135] E. Peli, J. Yang, R. Goldstein, and A. Reeves, "Effect of luminance on suprathreshold contrast perception," *Journal of the Optical Society of America A* **8**, pp. 1352–1359 (August 1991).

[136] M. Pope, H. Kallmann, and P. Magnante, "Electroluminescence in organic crystals," *Journal of Chem. Phys.* **38**, pp. 2042–2048 (1963).

[137] D. A. Reimann, M. J. Flynn, and J. J. Ciarelli, "System to maintain perceptually linear networked display devices," *SPIE Proc.* **2431**, pp. 316–326 (1995).

[138] O. W. Richardson, "On the negative radiation from hot platinum," *Proc. Camb. Phil. Soc.* **11**, p. 286 (1902).

[139] G. G. Roberts, M. McGinnity, W. A. Barlow, and P. S. Vincett, "Electroluminescence, photoluminescence and electroabsorption of a lightly substituted anthracene langmuir film," *Solid State Communications* **32**, pp. 683–686 (1979).

[140] J. W. Roberts and E. F. Kelley, "Measurements of static noise in display images," *SPIE Proc.* **4295**, pp. 211–218 (2001).

[141] S. P. Rogers, "Organic Electroluminescent Device Hermetic Encapsulation Package and Method of Fabrication," U.S. Patent No. 5,874,804 (1999).

[142] B. E. A. Saleh and K. Lu, "The Fourier scope: An optical instrument for measuring LCD viewing-angle characteristics," *Journal of the SID* **4(1)**, pp. 33–40 (1996).

[143] E. Samei, A. Badano, D. Chakraborty, K. Compton, C. Cornelius, K. Corrigan, et al., *Assessment of Display Performance for Medical Imaging Systems*, draft report of the American Association of Physicists in Medicine Task Group 18, Version 9.1 (2003).

[144] E. Samei and M. J. Flynn, "A method for in-field evaluation of the modulation transfer function of electronic display devices," *SPIE Proc.* **4319**, pp. 599–607 (2001).

[145] Samsung SDI Co., "SDI develops ultra fine high-speed LCD for handset," http://www.samsungsdi.co.kr (in Japanese and English), posted July 30, 2003.

[146] J. L. Sanford and F. R. Libsch, "TFT AMOLED pixel circuits and driving methods," *SID Tech. Dig.* **34**, pp. 10–13 (2003).

[147] T. Sasaoka, M. Sekiya, A. Yumoto, J. Yamada, T. Hirano, Y. Iwase, et al., "A 13.0-inch AM-OLED display with top emitting structure and adaptive current mode programmed pixel circuit (TAC)," *SID Tech. Dig.* **32**, pp.384–387 (2001).

[148] W. Schottky and J. Issendorff, "Quasineutrale elektrische diffusion im ruhenden und strömenden gas," *Zeitshrift für Physik* **31**, pp. 163–201 (1925).

[149] M. I. Sezan, K. L. Yip, and S. J. Daly, "Uniform perceptual quantization: applications to digital radiology," *IEEE Transactions on Systems, Man, and Cybernetics* **SMC-17(4)**, pp. 622–634 (1987).

[150] T. Shimoda, M. Kimura, S. Seki, H. Kobayashi, S. Kanbe, S. Miyashita, et al., "Technology for active matrix light emitting polymer displays," in *Proc. IEDM '99*, pp. 107–110 (1999).

[151] T. Shimoda, H. Ohshima, S. Miyashita, M. Kimura, T. Ozawa, I. Yudasaka, et al., "High resolution light emitting polymer display driven by low temperature polysilicon thin film transistor with integrated driver," *Proc. Asia Display '98*, pp. 217–220 (1998).

[152] G. Spencer, P. Shirley, K. Zimmerman, and D. P. Greenberg, "Physically based glare effects for digital images," in *Computer Graphics Proceedings, Annual Conference Series SIGGRAPH 95*, pp. 325–334 (1995).

[153] W. S. Stiles, "The effect of glare on the brightness difference threshold," *Proc. Royal Soc. London* **B104**, pp. 322–351 (1929).

[154] W. S. Stiles and B. H. Crawford, "The luminous efficiency of rays entering the eye pupil at different points," *Proc. Royal Soc. London* **122**, pp. 428–450 (1937).

[155] C. W. Tang and S. A. Van Slyke, "Organic electroluminescent diodes," *Applied Physics Letters* **51(12)**, pp. 913–915 (September 1987).

[156] S. Terada, G. Izumi, Y. Sato, M. Takahashi, M. Tada, K. Kawase, et al., "A 24-inch AM-OLED display with XGA resolution by novel seamless tiling technology," *SID Tech. Dig.* **34**, pp. 1463–1465 (2003).

[157] H. S. Tong and G. Prando, "Hygroscopic ion-induced antiglare/antistatic coating for CRT applications," *Proc. of the Society for Information Display* **23**, pp. 514–517 (1992).

[158] Toshiba Matsushita Display Technology Co., Ltd., "Toshiba Matsushita Display Technology introduces world's largest polymer organic light-emitting diode display," http://www.tmdisplay.com/tm_dsp/press/2002/04-16a.htm, posted April 16, 2002.

[159] T. Tsujimura, Y. Kobayashi, K. Murayama, A. Tanaka, M. Morooka, E. Fukumoto, et al., "A 20-inch OLED display driven by super-amorphous-silicon technology," *SID Tech. Dig.* **34**, pp. 6–9 (2003).

[160] N. Umezu, Y. Nakano, T. Sakai, R. Yoshitake, W. Herlitschke, and S. Kubota, "Specular and diffuse reflection measurement feasibility study of ISO 9241, part 7: method," *Displays* **19**, pp. 17–25 (1998).

[161] J. J. van Oekel, "Improving the contrast of CRTs under low ambient illumination with a graphite coating," *Proc. of the Society for Information Display* **26**, pp. 427–430 (1995).

[162] J. J. van Oekel, M. J. Severens, G. M. H. Timmermans, and A. A. M. Mouws, "Improving contrast and color saturation of CRTs by Al_2O_3 shadow mask coating, *Proc. of the Society for Information Display* **28**, pp. 436–439 (1997).

[163] P. S. Vincett, W. A. Barlow, R. A. Hann, and G. G. Roberts, "Electrical conduction and low voltage blue electroluminescence in vacuum-deposited organic films," *Thin Solid Films* **94**, pp. 171–183 (1982).

[164] H. Wakemoto, S. Asada, N. Kato, Y. Yamamoto, M. Tsukane, T. Tsurugi, et al., "An advanced in-plane switching mode TFT-LCD," *Proc. of the Society for Information Display* **26**, pp. 929–932 (1997).

[165] M. Weibrecht, G. Spekowius, P. Quadflieg, et al., "Image quality assessment of monochrome monitors for medical soft copy displays," *SPIE Proc.* **3031**, pp. 232–244 (1997).

[166] S. L. Wright, S. Millman, and M. Kodate, "Measurement and digital compensation of crosstalk and photoleakage in high-resolution TFTLCDs," *SPIE Proc.* **3636**, pp. 200–211 (1999).

[167] N. Yamada, S. Kohzaki, F. Funada, and K. Awane, "A full-color video-rate anti-ferroelectric LCD with wide viewing angle," *Proc. of the Society for Information Display* **17**, pp. 789–792 (1995).

[168] Y. Yang and S. C. Chang, "Pyramid-shaped pixels for full-color organic emissive displays," *Applied Physics Letters* **77(7)**, pp. 936–938 (2000).

[169] G. Yu, H. Nishino, A. J. Heeger, T. A. Chen, and R. D. Rieke, "Enhanced electroluminescence from semiconducting polymer blends," *Synthetic Metals* **72**, pp. 249–252 (1995).

[170] C. Zhang, H. Von Seggern, B. Kraabel, H. W. Schmidt, and A. J. Heeger, "Blue emission from polymer light-emitting diodes using non-conjugated polymer blends with air-stable electrodes," *Synthetic Metals* **72**, pp. 185–188 (1995).

[171] K. Ziemelis, "Display technology: glowing developments," *Nature* **399**, pp. 408–411 (2000).

[172] S. M. Zimmerman, G. W. Jones, and H. E. Webster, "Sealing Structure for Organic Light Emitting Devices," U.S. Patent No. 6,198,220 (May 2001).